

**CHARACTERISTICS OF DEFORMATION BANDS IN POORLY LITHIFIED
SAND: RIO GRANDE RIFT, NEW MEXICO**

by

James Matthew Herrin

Submitted in Partial Fulfillment
of the Requirements for the Degree of
Master of Science in Geology

New Mexico Institute of Mining and Technology
Department of Earth and Environmental Science

Socorro, New Mexico

May, 2001

ABSTRACT

Faults and fault zones, even those accommodating small amounts of displacement, can either facilitate or hinder fluid flow. The hydraulic properties of a fault zone depend largely on the character and geometry of the structural elements constituting the fault zone. The widespread occurrence of faulted sediments in aquifers and petroleum reservoirs warrants a better understanding of sediment deformation, yet few systematic studies have addressed faults that cut unlithified sediments. In this study, small-displacement normal faults that cut Tertiary sand and conglomerate have been characterized through outcrop mapping, petrographic observation, and electron microprobe imaging and analysis. Displacement across most of the 32 faults studied ranges from 0.1 to at least 1.5 meters; one fault records a minimum of 6.4 meters of throw. Nearly all faults in the hanging wall of the latter large-displacement fault are subparallel to it, whereas conjugate fault sets are common in the footwall. Where it cuts conglomerate, each fault consists of a 1-10 cm wide shear zone that has a finer grain size than the protolith and includes fractured clasts. Where faults cut partially lithified sand they are composed of multiple deformation bands arranged in simple to geometrically complex arrays. The most complex arrays are found in faults recording displacement greater than one meter; in general, however, the geometric characteristics of these arrays are not predicated on either fault displacement or location relative to larger-displacement

faults. The width of the deformation band fault zones is least at conglomerate-sand contacts and increases with increasing distance from these contacts. In contrast to previous laboratory and field studies of deformation bands in sandstone, these arrays do not show a linear increase in number of deformation bands with increasing displacement.

Deformation bands are distinguished in thin section by a decrease in macroporosity and an abundance of brown fine-grained matrix relative to undeformed protolith. Porosity within deformation bands is chiefly in the form of microporosity, defined by pore diameters <0.5 microns. Petrographic point count data and scanning electron micrographs show that the brown matrix material is created through the preferential comminution of lithic fragments and feldspar grains. Quartz grains are also fractured, but to a lesser degree. Production of this fine-grained pseudomatrix results in a five-fold reduction in mean pore size as well as porosity. Grain rotation is evident near the boundaries of deformation bands, where elongate grains have been rotated into the plane of the deformation band. This alignment is also evident within the deformation band.

The decrease in porosity and reduction in pore size within deformation bands indicate these structures should influence fluid flow. Previous studies show that under saturated conditions, deformation bands that cut unlithified or partially lithified sand will act as low-permeability barriers to fluid flow, whereas under unsaturated conditions they may act as preferential flow paths for the wetting phase.

ACKNOWLEDGMENTS

This research was supported in part by funding from National Science Foundation, Hydrologic Sciences program grant #EAR-9614385, and by the New Mexico Geological Society. I would like to thank the Bosque del Apache National Wildlife Refuge and the Burlington Northern Santa Fe Railroad for granting access to the study site.

A number of individuals provided assistance with field work, field equipment, and laboratory procedures. These include New Mexico Tech students John Sigda, Geoffrey Rawling, Chris Dimeo, Peter Rinkleff, and New Mexico Bureau of Mines and Mineral Resources (NMBMMR) staff members Lynn Heizler, Dr. Nelia Dunbar, and Dr. David Love. Several geologists visited my outcrop, viewed my samples and thin sections, and provided valuable commentary and feedback on this research: Drs. Harold Tobin and Lawrence Teufel (New Mexico Tech), Drs. Steve Cather and Richard Chamberlain (NMBMMR), Dr. John Lorenz (Sandia National Laboratories), Marlon Downey and Dr. Dave Stearns (University of Oklahoma), Dr. Steve Laubach (Texas Bureau of Economic Geology), Dr. George Davis (University of Arizona), Dr. Atilla Aydin (Stanford University), and Dr. Craig Forster (Utah State University).

Most of all I would like to thank the members of my graduate committee: Drs. Laurel Goodwin, Peter Mozley, and John Wilson; and Dr. Dave Johnson, Dean of Graduate Studies.

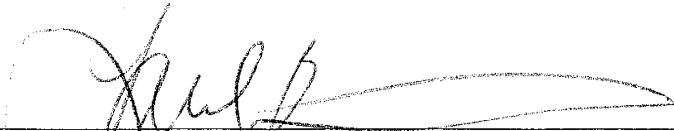
TABLE OF CONTENTS

ACKNOWLEDGMENTS	ii
TABLE OF CONTENTS	iii
LIST OF FIGURES AND TABLES	iv
INTRODUCTION	1
PREVIOUS STUDIES OF DEFORMATION BANDS	7
GEOLOGIC SETTING AND STUDY SITE LOCATION	11
METHODS	14
Outcrop Study	14
Petrographic Study	15
RESULTS	17
Stratigraphy Exposed at Canyon Trail Site	17
Faults at the Canyon Trail Site	18
Petrographic Observations	32
DISCUSSION	45
Age and Character of Faulting	45
Development of Deformation Band Arrays	45
Compositional Controls on Deformation	50
CONCLUSIONS	52
REFERENCES CITED	55
APPENDIX A	61
APPENDIX B	62

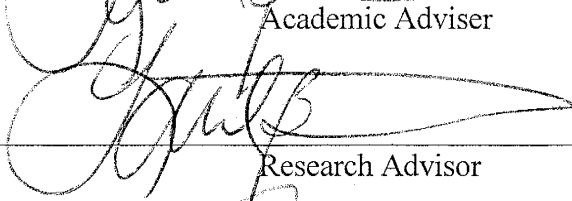
LIST OF FIGURES AND TABLES

Figure 1: Alluvial basins of western U.S.A.	2
Figure 2: Application of fault/fluid flow studies	4
Figure 3: Study site location	13
Figure 4: Principal fault locations	19
Figure 5: Canyon Trail, west face schematic	21
Figure 6: Displacement versus distance plots	23
Figure 7: Photo, fault in conglomerate	24
Figure 8: Fault zone width characteristics	25
Figure 9: Photo, deformation band outcrop appearance	27
Figure 10: Photo, wetting of deformation bands	28
Figure 11: Deformation band array variety	29
Figure 12: Photo, zone of deformation bands	30
Figure 13: Array property plots	33
Figure 14: Array property plots	34
Figure 15: Deformation band dip distribution	35
Table 1: Point Count Data	36
Figure 16: Thin section composite photomicrograph	38
Figure 17: Ternary plot, pore space evolution	39
Figure 18: BSE images	41
Figure 19: Photomicrograph, fractured grains	43
Figure 20: Grain orientation data	44

This Thesis is accepted on behalf of the faculty
of the Institute by the following committee:



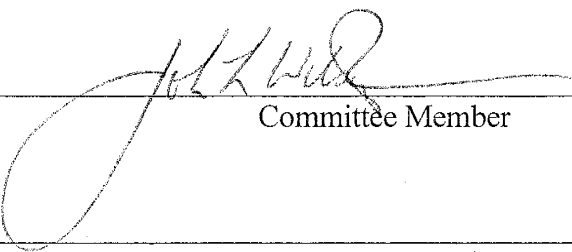
Academic Adviser



Research Advisor



Committee Member



Committee Member



Committee Member

26 April 2001

Date

INTRODUCTION

Determining whether faults act as seals, conduits, or complex seal/conduit systems in the earth's subsurface is of great interest for economic and environmental reasons. Understanding how faults trap, conduct, or impede fluid flow is important for the exploration of hydrocarbons and for the efficient development of existing oil and gas fields. Similarly, problems concerning the transport of gases, non-aqueous phase liquids, or contaminated groundwater often depend on a keen awareness of fault hydrologic properties. To obtain a better understanding of fault properties with respect to fluid flow, many workers in the past two decades have focused their attention on porosity and permeability characteristics of faults cutting various lithologies, and have examined the physical and chemical processes responsible for altering the porosity and permeability of faults and fault zones (e.g., Pittman, 1981; Knipe, 1993; Antonellini and Aydin, 1994; Caine et al., 1996; Hippler, 1997; Yielding et al., 1997).

Much of the research concerning fault characteristics has been directed at faults that cut crystalline or lithified sedimentary rocks. Only recently have unlithified or partially lithified sediments received attention. This deficiency in the literature is not due to the absence or triviality of faults in sediments, for faults cutting thick sections of sediments are observed in many tectonic settings, and they crosscut many aquifers and petroleum reservoirs. In the continental U.S. alone, alluvial basins cover 1,025,000 km² from Texas to the Pacific Northwest (Heath, 1984). Nearly all of this area coincides with regions of active tectonism (e.g., Basin and Range Province, Rio Grande Rift, San Andreas Fault Zone; Figure 1). Groundwater is the dominant water source in these regions, with aquifers consisting of thick sections (100s to 1,000s of meters) of unlithified or partially lithified sediment. The rapid growth of urban areas which rely on this

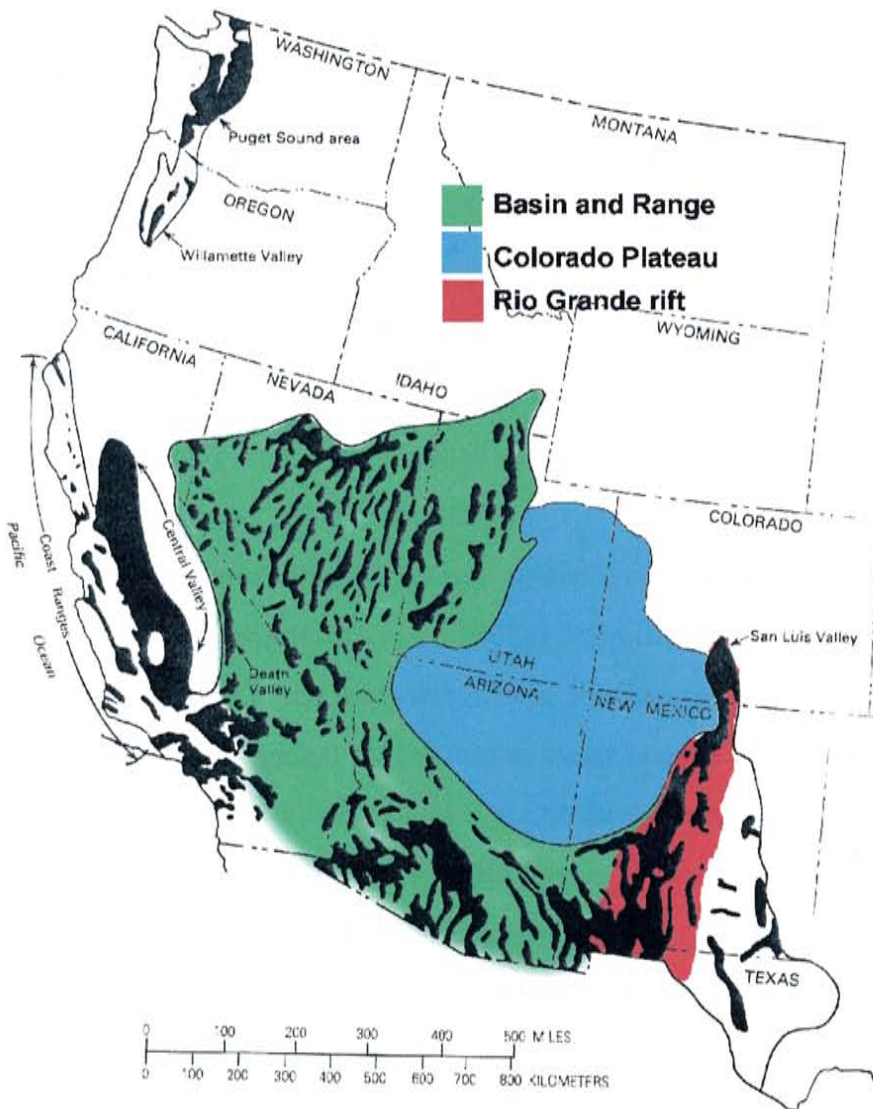


Figure 1: Map of western United States showing distribution of alluvial basins (black fill) within tectonically active physiographic provinces. Many of these basins serves as aquifers for municipal water supplies. Modified from Heath (1984) and Stanley (1989).

groundwater supply (e.g., Las Vegas, NV; Albuquerque, NM; Phoenix, AZ) and the development of radioactive waste repositories in the region (e.g., Yucca Mountain, NV; Waste Isolation Pilot Plant, NM) illustrate the need for a better understanding of fluid/fault interaction in poorly lithified materials. Economic concerns over petroleum production in hydrocarbon reservoirs which are composed of young unlithified sediments have promoted more detailed fault studies within the Gulf of Mexico, the North Sea, and the Niger River Delta (e.g., Smith, 1980; Bouvier et al., 1989; Hardmann and Booth, 1991; Nybakken, 1991; Knott, 1993; Hippler, 1997). Motivated by these concerns, some workers have begun characterizing the hydrologic properties of faulted sediments. Laboratory and in-situ permeametry studies of poorly lithified sand have demonstrated that even small faults may reduce the saturated permeability to as little as 1/10,000th of its original permeability (Sigda, 1997; Hong, 1999).

In order to better predict the hydrologic influence of faults in aquifers and reservoirs (whether composed of rock or unlithified sediment) and to estimate the permeability characteristics of the faults themselves, it is necessary to view the problem at several scales (Figure 2). Regional studies seek to locate major faults, determine their orientation, and identify their distribution pattern. These data coupled with stratigraphic information may be used to identify “juxtaposition seals”, where faults juxtapose high permeability reservoir rock against low permeability non-reservoir rock. Most faults are zones of deformation consisting of some combination of smaller faults, fractures, breccia, and gouge in addition to discrete planar slip surfaces. At this smaller scale, one would like to know something of the fault zone architecture – how smaller secondary faults and fractures are distributed, how they are connected, total width of the zone, etc. (e.g., Hippler, 1993; Antonellini and Aydin, 1995; Caine et al., 1996). Finally, grain-scale observations are needed to understand how deformation and diagenesis enhance or degrade the porosity and permeability of the fault material itself. Thus a complete study aimed at understanding how faults affect the flow of fluids in a reservoir or aquifer requires data from many sources and scales of observation.

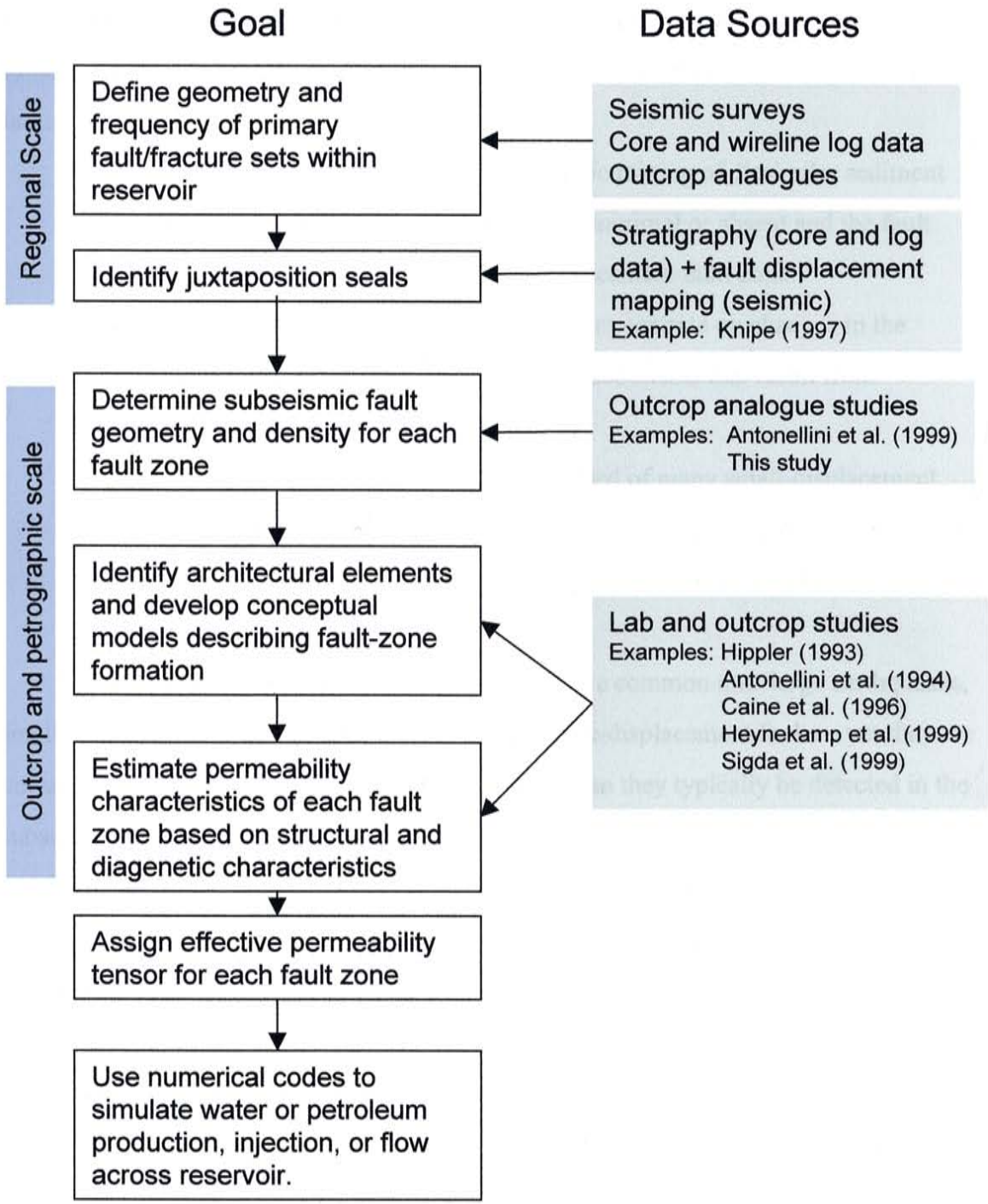


Figure 2: Flow chart illustrating ideal process for incorporating fault/fracture permeability characteristics into an aquifer or reservoir flow model.

In this thesis I describe outcrop and grain-scale observations of uncemented small-displacement (<3 m) faults that cut poorly lithified sand and conglomerate in central New Mexico. There are several advantages to focusing on uncemented small-displacement faults:

- With a restricted amount of slip, tectonic mixing of dissimilar sediment from multiple stratigraphic intervals is minimal or absent and the fault zone is less complex than a large-displacement fault zone.
- The absence of cements allows one to concentrate on changes in the petrophysical characteristics of faulted sediments that result from deformation alone.
- Larger fault zones are typically composed of many small-displacement faults, so studying the properties of these basic building blocks may enable one to predict the effective hydraulic properties of an arbitrarily complex fault zone.

Additionally, just as small earthquakes are more common than large earthquakes, small-displacement faults are more common than large-displacement faults – yet they are not usually included on standard geologic maps, nor can they typically be detected in the subsurface with geophysical techniques (Walsh and Watterson, 1991; Carter and Winter, 1995). Previous workers demonstrate that even faults with displacements on the order of centimeters can greatly reduce permeability (Antonellini and Aydin, 1994; Sigda et al., 1999), and such faults have been blamed for production difficulties in many petroleum reservoirs (L. Teufel, personal comm., 1999)

Finding relationships among such properties as fault displacement, fault density, and position relative to other faults (or confirming the lack of such relationships) has many potential applications. For instance, a 15-meter displacement of strata caused by a fault may be detected with industry-standard seismic reflection or refraction methods, but adjacent, smaller faults related to the same system would be invisible using the same method. If small-displacement faults play an important role in the plumbing system of an

aquifer or petroleum reservoir, but only faults with displacements greater than 15 meters can be detected remotely, it would be extremely helpful if one could predict the location and density of the secondary faults with respect to the larger faults. Alternatively, in some situations it may be desirable to predict the location of a large, unexposed fault based on the characteristics of smaller related faults. For example, Robin Pearson (written comm., 2000) used the small fault density profile associated with a large-displacement fault to infer its location where it was not exposed.

In this study, I examined relationships between small-displacement fault-zone geometry and such factors as magnitude of displacement, sediment composition, and location relative to other faults. In addition, I evaluated 1) how the porosity, composition, and fabric of the undeformed parent sediment were modified by small-displacement faults and 2) which deformation mechanisms and diagenetic processes were responsible for altering fault porosity. The primary results of this study are as follows:

- These faults are expressed as shear zones where they cut conglomerate, and arrays of deformation bands where they cut sand. (Deformation bands are small-displacement faults characterized by reduced grain size and porosity; Aydin, 1978).
- Deformation band arrays vary in width and geometric complexity, but no simple relationship can be found between geometry or width and factors such as total fault-zone displacement or proximity to moderate-displacement faults. This is not consistent with previous deformation band studies in lithified sandstones, which indicate a direct relationship between fault displacement and fault-zone width.
- Grain-size reduction and pore collapse within deformation bands reduces total porosity. Small pore and grain size within deformation bands may facilitate nucleation of cement, resulting in a further decrease in porosity.

PREVIOUS STUDIES OF DEFORMATION BANDS

Deformation bands are narrow (1-3 mm) shear zones which accommodate small displacements (< 5 cm) in porous rock and sediment (see Antonellini and Aydin, 1995), and references therein). Deformation is accommodated by compaction and/or cataclastic flow within a deformation band. They are particularly well developed in high porosity quartz arenites (as compared to other sedimentary rocks) where they typically appear as whitish bands which project in positive relief from weathered surfaces – similar in appearance to mineralized fractures. As early as 1918, geologists noted the presence of these vein-like structures in faulted sandstone, and Heald (1956) correctly identified them as zones of cataclasis. They have been studied in experimentally deformed rock since 1973 (Friedman and Logan, 1973) where they were termed “Lüders’ lines” or “Lüders’ bands”, a reference to similar deformation structures formed in soft steel, described in the mid-19th century. Still, most field geologists probably identified them as veins until the late 1970's and early 1980's when work by Aydin (1978), Aydin and Johnson (1978), Pittman (1981) and Jamison and Stearns (1982) brought them to the attention of the geologic community. They have been called microfaults, gouge zones, granulation seams, cataclastic bands, shear bands, disaggregation bands, or simply faults (Pittman, 1981; Jamison and Stearns, 1982; Underhill and Woodcock, 1987; Steen and Andresen, 1999; Knipe, personal comm., 2000) Aydin (1978) called these structures “deformation bands”, and this remains the preferred term among structural geologists today.

Aydin (1978) described deformation bands common in porous quartz arenites. Each band consists of a cataclastic core characterized by low porosity and fine grain size surrounded by a zone of reduced porosity with respect to the protolith, but less cataclasis

than the deformation band core. More recent studies have added more members to the deformation band family, and some geologists have created classification systems based on deformation band microstructures and/or geometry. That of Antonellini et al. (1994) identified three main groups and seven subgroups of deformation bands based on the presence and extent of cataclasis and clay smear (clay minerals dragged into the shear zone from argillaceous strata). Mollema and Antonellini (1996) added compaction bands – deformation bands with no shear offset formed perpendicular to the maximum compressive stress – to the list. Fossen and Hesthammer (1997) used the terminology of Walsh and Watterson (1991) to categorize systems of deformation bands based on how they are linked (i.e. “soft-linked” versus “hard-linked”). Finally, Davis (1999) offered a classification system using a combination of microstructures and meso-scale geometry.

Deformation bands may cluster locally around structures where they accommodated fault or fold deformation (e.g., Jamison and Stearns, 1982) or may be distributed regionally as a consequence of burial compaction (Davis, 1999). Observations that meter-scale displacement in porous sandstone is distributed across zones of deformation bands, within which each individual deformation band accommodated a limited amount of slip, has led many to conclude that deformation bands exhibit strain-hardening behavior. Many geologists hypothesize that during the development of a deformation band, pore collapse and greater grain-to-grain contact area cause strain-hardening (Jamison and Stearns, 1982; Antonellini et al., 1994). After a finite amount of deformation, less energy is required to create a new deformation band than to continue displacement along the original band. Additional deformation may also be accommodated through a loss of cohesion and creation of a slip surface or “classic” fault. Aydin and Johnson (1978) used field evidence to support their hypothesis that failure on slip surfaces accommodating meters of displacement was preceded by the accumulation of deformation bands in the proto-footwall. Thus, prior to the creation of a slip surface, there should be a direct correlation between total fault displacement and the number of bands associated with that fault (Antonellini and Aydin, 1995). Mair et al. (2000)

confirmed this relationship in laboratory studies of faulted quartz arenites.

Deformation bands are typically less porous and permeable than the host rock or sediment. Antonellini and Aydin (1994) cite deformation band porosity values one order of magnitude lower, and permeability values three orders of magnitude less, than the undeformed host rock. Capillary pressure within these bands may be 100 times greater than the host. Thus deformation bands may pose serious obstacles to oil, gas, or water extraction. Even if they aren't capable of sealing large columns of fluid over geologic time scales, on a human time scale they may act as baffles or barriers to non-wetting phases (Downey, 1984; Antonellini and Aydin, 1994).

Deformation bands that cut porous quartz arenites such as the Navajo, Wingate, and Entrada sandstones of the Colorado Plateau have been the subject of most deformation band studies (e.g., Aydin, 1978; Jamison and Stearns, 1982; Davis, 1999). Structural, microstructural and diagenetic evidence suggests a pre-lithification origin for deformation bands found in some rocks (Antonellini et al., 1994; Swierczewska and Antoni, 1998). Deformation bands are indeed found in many fault zones cutting unlithified or partially lithified sediments, and recent studies have begun to assess their permeability characteristics, grain size distribution, and microstructures (e.g., Mozley and Goodwin, 1995; Goodwin and Haneberg, 1996; Sigda et al., 1999; Cashman and Cashman, 2000). For example, Goodwin and Haneberg (1996) noted that elongate sand grains were aligned within zones of deformation bands, producing a roughly fault-parallel foliation and slip-parallel lineation. Sigda (1997) and Hong (1999) describe geometric features of deformation band arrays in faulted sands in central New Mexico virtually identical to those found in lithified sandstone. Deformation bands in sand exhibit a reduction in both overall porosity and pore size with respect to the protolith. As mentioned previously, the permeability of the host sand is reduced by these deformation bands (Hong, 1999; Sigda et al., 1999). Sigda et al. (1999) also surmised that smaller pore sizes within a deformation band may result in an increased unsaturated hydraulic conductivity, especially when the soil moisture content is sufficiently low due to pore size

reduction and an increase in the importance of capillary forces. This would result in an increased fluid flux along the deformation band, effectively creating fast paths for fluid movement through the vadose zone.

GEOLOGIC SETTING AND STUDY SITE LOCATION

The study area is located in central New Mexico near the southern boundary of the Socorro Basin – one of a number of north-trending sedimentary basins associated with the Rio Grande rift (Chapin and Cather, 1994). This intracontinental rift extends from southern Colorado to northern Mexico, is bounded on the west by the Colorado Plateau and on the east by the continental craton, and consists of a chain of alternating east- and west-tilted half grabens (Figure 1; Kelley, 1982). Like the Basin and Range physiographic province, the Rio Grande rift is characterized by high heat flow, thin crust, and shallow seismicity (Russell and Snelson, 1994). The Socorro Basin, bounded on the north by the Albuquerque-Belen Basin and on the south by the San Marcial and Jornada del Muerto basins, coincides with an abrupt broadening of the rift. Extension increases from 30% to 50% as the rift trends southwestward around the Colorado Plateau and merges with the Basin and Range province to the west. Rifting in this area began in latest Oligocene or early Miocene time with the creation of the Popatosa Basin (Chapin and Cather, 1994). Uplift of the Chupadera-Socorro-Lemitar range 9-10 m.y. ago divided this basin into the La Jencia and Socorro basins (Cather et al., 1994). The main synrift, basin-filling unit is the Oligocene-Pliocene Santa Fe Group. The Lower Santa Fe Group, which is cut by the faults in the study area, consists of intertonguing sand (eolian, fluvial, and alluvial fan deposits), gravel, and fine-grained basin floor deposits, and represents deposition prior to the development of an extra-basinal drainage system (Lozinsky et al., 1991). Structural relief of the Socorro basin is approximately 3 km. Present day seismic activity is chiefly in the form of microearthquakes (magnitude < 3.0) created as a result of dip-slip movement on north-striking normal faults (Sanford, 1978).

The study site is located in the southern portion of the Socorro Basin

approximately 30 kilometers south of the city of Socorro, within the Bosque del Apache National Wildlife Refuge (Figure 3). In this area relatively flat-lying sand, gravel, and conglomerate deposits of the Popatosa Formation (Lower Santa Fe Group) are exposed in canyon walls, arroyos, road cuts, and railroad cuts. The sands and gravels of the Popatosa here represent alluvial fan, transitional fan, and eolian facies (Regina Rone, written comm., 1999). Several gravel and sand units are interbedded in this area, and a simplified stratigraphic sequence consists of four main units: Lower Sand, Lower Gravel, Upper Sand, Upper Gravel (Robin Pearson, written comm., 2000). Some laminae and thin beds within the sand units are cemented, and elongate calcite concretions protrude from many outcrops, but generally the sands are not cemented. They are cohesive enough to create vertical faces and overhangs, but can be easily excavated with a trowel. The gravel beds are moderately well indurated, and I use the term conglomerate to describe them in this paper. In addition to providing good exposures of the stratigraphy, railroad cuts reveal numerous normal faults. A particularly well exposed northeast-trending cut (hereafter referred to as the Canyon Trail site) intersects a relatively dense cluster of faults, and was selected as the site for this study.

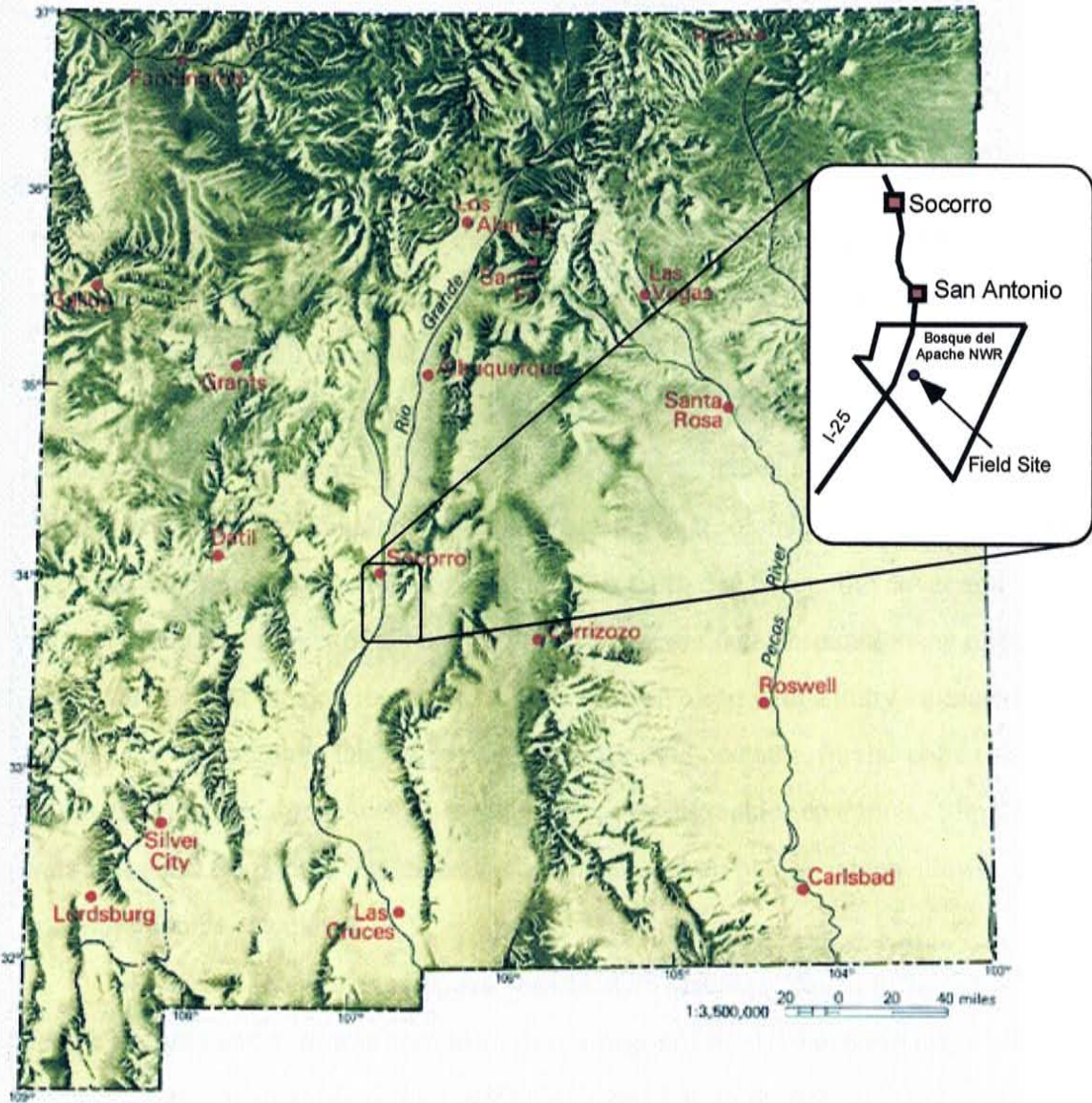


Figure 3: Field site location within the Rio Grande rift, approximately 30 km south of Socorro, NM.

METHODS

Outcrop Study

The locations of fault zones were recorded using a digital theodolite by surveying the point at which each fault trace intersected the ground surface in the railroad cut. In order to capture the geometric complexity of the deformation band arrays, the lower portions of many fault zones were sketched on mylar sheets at a scale of 1:10 (Appendix B). To aid in accurate mapping I used a 1-meter by 70-centimeter frame which was subdivided into a 1-decimeter string grid. The grid was nailed to the outcrop face with the short side leveled horizontally. It was not possible to accurately map some fault zones, especially those near the moderate-displacement fault, due to regolith cover and cavitation of the outcrop. A veneer of silt and clay on the outcrop face obscured many of the smaller faults, so much of the outcrop face had to be scraped clean with a putty knife and paint brush prior to mapping. Displaced conglomerate-sand contacts, fluvial-eolian sand contacts, and clay laminae were used to measure stratigraphic separation. Slip direction was measured from grain lineations visible on some fault planes, which allowed net slip magnitude to be calculated.

A personal computer equipped with SCION Image (National Institutes of Health) image analysis software was used to analyze images of the 1:10 outcrop maps. Images were processed to quantify certain deformation band array properties in order to evaluate relationships between deformation band array geometry and factors such as fault displacement or distance of the array from the large-displacement fault. Individual sketch panels (measuring 10 cm tall by 7 cm wide) were scanned to create a digital image. Each digital image was cropped to equal pixel dimensions, and any annotations or stray markings were digitally erased. A thresholding function converted the grayscale image to

a binary format (i.e., an image in which each pixel is either black or white). Total deformation band material in each sketch panel was estimated by dividing the number of black pixels by the total number of pixels. In order to analyze fault segment orientation and intersection characteristics, a further processing step was needed. A “skeletonizing” algorithm reduced each identified line segment to one-pixel width. Intersections were identified, and an image of intersection points was stored in a separate file. Subtracting this intersection image from the original resulted in a skeletonized image of the fault array in which all intersections were broken. A pre-programmed routine fitted an ellipse to each line segment. The angle between the major axis of this ellipse and the horizontal was used to determine fault segment apparent dip. The value obtained by dividing the number of intersections by total length of deformation band material was used as an indicator of array complexity.

Petrographic Study

Due to the friable nature of the sand in this area, preparation of samples for thin-section analysis required special procedures developed by Chris Dimeo (pers. comm., 1997). Samples were carefully removed from the outcrop using a 3-inch diameter hole saw. After being left to dry in an oven for two days, the cores were saturated with a low viscosity blue-dyed epoxy, and placed in a bell jar under vacuum for two days while the epoxy cured. Standard uncovered thin sections were then made from the cores. Microstructural analysis was focused on sand; no samples were taken from the conglomerate units.

Thin sections were examined first with a binocular Nikon petrographic microscope equipped with a mechanical stage. I used a standard point count procedure on selected thin sections to measure the abundance of the following constituents: quartz, plagioclase feldspar, potassium feldspar, undifferentiated lithic fragments, calcite, clay-size fraction, macroporosity, and microporosity. Minor constituents, such as pyroxenes, micas, and opaque oxides, were assigned to a single “Other” category. Microporosity is

defined by pore diameters < 0.5 microns and is identified in thin section by an apparently unresolvable mixture of pore and grain area (Mozley, 1999). All thin sections counted contained some portion of fault material as well as relatively undisturbed sediment. 300 points were counted within the undisturbed regions, and 150 points were counted in the areally smaller fault portion of each thin section.

In order to better understand grain-scale deformation processes and potential compositional changes facilitated by deformation, selected thin sections were polished for imaging and analysis on a Cameca SX-100 microprobe located at the New Mexico Bureau of Mines and Mineral Resources. With a beam current of 1 nanoamp and accelerating voltage of 25 kilovolts, backscattered electron images were collected at various levels of magnification, and nine elemental X-ray maps were collected from one location.

RESULTS

The intended goal of my outcrop and petrographic observations was to answer several questions:

- How is displacement accommodated by faults cutting poorly lithified sand?
- How are small-displacement, secondary faults related to larger-displacement faults?
- How is fault-zone architecture related to displacement?
- How do these fault zones grow?
- What deformation mechanisms are involved, and how do they modify the petrophysical characteristics of the faulted sediment?

As mentioned previously, in order to answer these questions and apply them to problems of fluid flow it is necessary to make observations at several scales. I open this section by presenting my outcrop-scale characteristics: first at a scale in which each fault may be considered a single plane, and second at a smaller scale at which each fault is represented by a zone comprising many smaller faults. Finally I will describe the evidence of grain-scale processes I observed with a petrographic microscope and electron microprobe.

Stratigraphy Exposed at Canyon Trail Site

The railroad cut at the Canyon Trail site exposes a length of approximately 140 meters of sand and conglomerate. Most of the detailed observations reported here come from the lower, roughly vertical walls of the exposure, which in some places rise up to 6 m above ground level. At this elevation, the northern half of the outcrop exposes the

Lower Gravel Unit whereas the southern half exposes eolian and fluvial sand mantled by a layer of conglomerate (Upper Sand and Upper Gravel Units).

The Lower Gravel Unit is poorly sorted, clast supported, and has rounded to subangular clasts. Clast diameters range from 30 cm to 1 cm, and are chiefly volcanic with lesser amounts of plutonic and chert clasts. At this outcrop, the Upper Gravel Unit is identical to the Lower, making stratigraphic correlations to other outcrops difficult (Robin Pearson, written comm., 2000). The Upper Sand Unit contains thick buff-colored beds of both eolian and fluvial deposits. The eolian sands show large scale, high-angle cross stratification whereas the fluvial sands show few sedimentary structures. Within the eolian deposits one may find small, spatially restricted, interdune deposits of laminated silt and clay. These deposits make up a very small percentage of the overall stratigraphy exposed at the Canyon Trail site. Isolated, thin (< 3 mm) laminae of pinkish or rust-colored silt and clay are found within both eolian and fluvial sand units. These typically mark an unconformity or depositional hiatus as evidenced by an abrupt change in grain size or mismatched cross bed sets on either side of the lamina. Calcite cement occurs in laterally restricted thin beds of sand, and elongate calcite concretions dot the outcrop, but nowhere at the Canyon Trail site have these concretions coalesced to form a laterally extensive cemented bed.

Faults at the Canyon Trail Site

Thirty-two normal faults were surveyed along the western side of the cut and twenty-five along the east (Figure 4). Nearly all of these faults strike northwest, with an average strike of 145° , and dip both northeast and southwest. Southwest-dipping faults are more numerous (Figure 5) and have an average dip of 65° S. North-dipping faults have an average dip of 72° . Lineations defined by oriented elongate sand grains were visible on many fault surfaces. Goodwin and Haneberg (1996) demonstrated that similar lineations record the direction of slip in a large-displacement fault in poorly lithified sediments, a conclusion that is supported by observations detailed in this thesis.

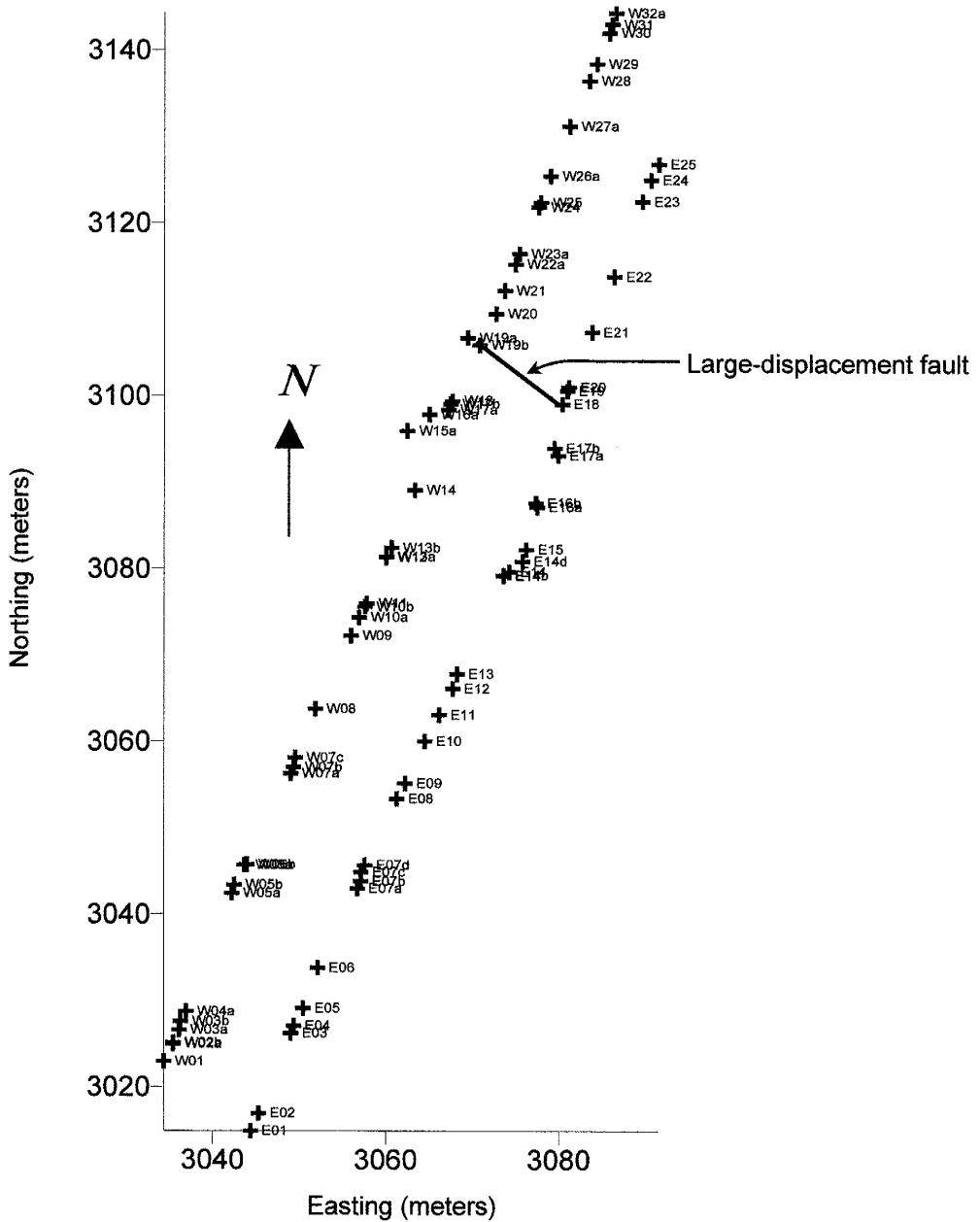


Figure 4: Map view of fault locations at Canyon Trail site. Crosses mark the location at which each principal fault intersects the ground surface. Although the cut is little wider than the standard-gauge railroad grade running through it, changes in each fault's displacement and geometry make it difficult to correlate faults across the cut.

Orientation measurements of these lineations indicate nearly pure dip-slip movement; local strike-slip components are consistently left-lateral (Figure 5).

Displacement of one fault often occurs where two faults intersect. Occurrences of north-dipping faults that cut south-dipping faults are approximately equal in number to south-dipping faults that cut north-dipping faults, indicating the contemporaneity of these two fault sets, and suggesting that these are conjugate sets. The average acute angle formed by the conjugate sets is 42° . The acute bisector dips approximately 86° to the southwest, suggesting this region (or at least the local area including the Canyon Trail outcrop) may have been rotated a few degrees to the northeast.

The largest displacement fault juxtaposes the Upper Sand and Upper Gravel units in the hanging wall against the Lower Gravel and Upper Sand units in the footwall. The absence (due to erosion) of a distinct marker bed or piercing point on both sides of this fault (hereafter referred to as the large-displacement fault) makes exact measurement of displacement impossible, but a minimum throw of 6.5 meters was established. This estimate is based on the vertical distance between the sand-conglomerate contact in the hanging wall and the top of the outcrop in the footwall. Four faults in the hanging wall adjacent to the large-displacement fault record displacements on the order of 1.5-3 meters, resulting in a minimum total displacement of approximately 15 meters within a 20-meter section of outcrop. Most of the other faults at the Canyon Trail site record displacements of 0.1-1.5 meters. Immediately north of the large-displacement fault the contact between conglomerate and overlying sand is hidden by regolith and vegetation, hindering displacement measurement.

A plot of fault location versus displacement shows a relationship between displacement and position from the large-displacement fault in the hanging wall (Figure 6a). Among the faults in the hanging wall of the large-displacement fault, there is a general increase in displacement with increasing proximity to the large-displacement fault. However, among the faults in the footwall of the large-displacement fault there appears to be no relationship between displacement and position relative to the large fault

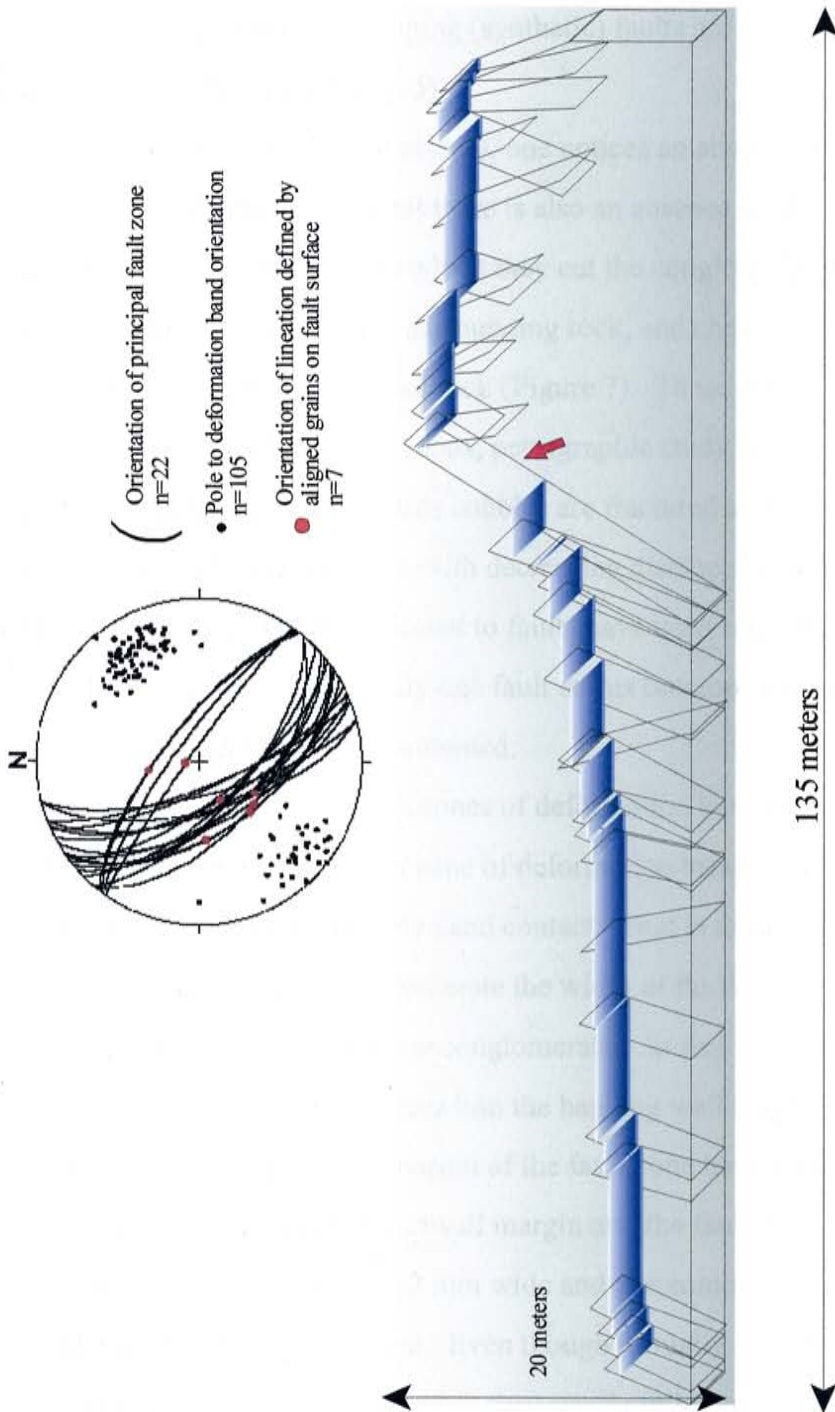


Figure 5: Diagrammatic illustration of west outcrop face (looking northwest) at the Canyon Trail site showing principal fault zones. Lower hemisphere equal area net at top shows orientations of principal fault planes, poles to deformation bands, and grain lineations. Blue layer is used to show measured displacement of each fault, but does not represent a particular stratigraphic contact. Only a minimum amount of displacement could be estimated for the fault indicated by the red arrow due to erosion of the outcrop. Displacements for faults to the right (north) of this main fault were actually measured at ground level.

(Figure 6). Within the study site there is no decrease in fault density with increasing distance from the large-displacement fault in either the footwall or the hanging wall. Nearly all faults in the hanging wall of the large-displacement fault dip to the southwest, synthetic to the large-displacement fault, whereas in the footwall northeast-dipping (antithetic) and southwest-dipping (synthetic) faults are nearly equal in number as well as displacement magnitude (Fig. 5).

Looking at each fault closely, one notices an absence of open fractures. Except for the large-displacement fault there is also an absence of discrete slip surfaces. Faults are shear zones 1-10 cm wide where they cut the conglomerate units, slightly recessive in outcrop profile relative to the surrounding rock, and characterized by a smaller and more uniform grain size than the host rock (Figure 7). These shear zones may, in fact, be narrow zones of deformation bands; petrographic study would be necessary for complete characterization. In many places cobbles are fractured and the frequency of fractured cobbles qualitatively increases with decreasing distance from the fault. Also, many cobbles and large pebbles adjacent to faults have been rotated so that their long axes are parallel to the fault plane. Only one fault at this outcrop (intersecting survey points W08 and E09 in Figure 4) is well cemented.

Faults are expressed as zones of deformation bands where they cut sand units (Figure 8). The width of each zone of deformation bands increases with increasing distance from the conglomerate-sand contact. That is to say, at the contact between a sand unit and overlying conglomerate the width of the deformation band array in the sand is comparable to its width in the conglomerate. As one follows the array down dip, in the direction of slip, the zone widens into the hanging wall (Figure 8). The deformation bands near the hanging wall margin of the fault zone have a shallower dip than both deformation bands near the footwall margin and the fault zone in the conglomerate unit. Each deformation band is 1.5-2 mm wide and accommodates a small amount of displacement, usually 1-30 mm. Even though virtually all deformation bands at the Canyon Trail site are not cemented, they stand out in positive relief from the host sand on

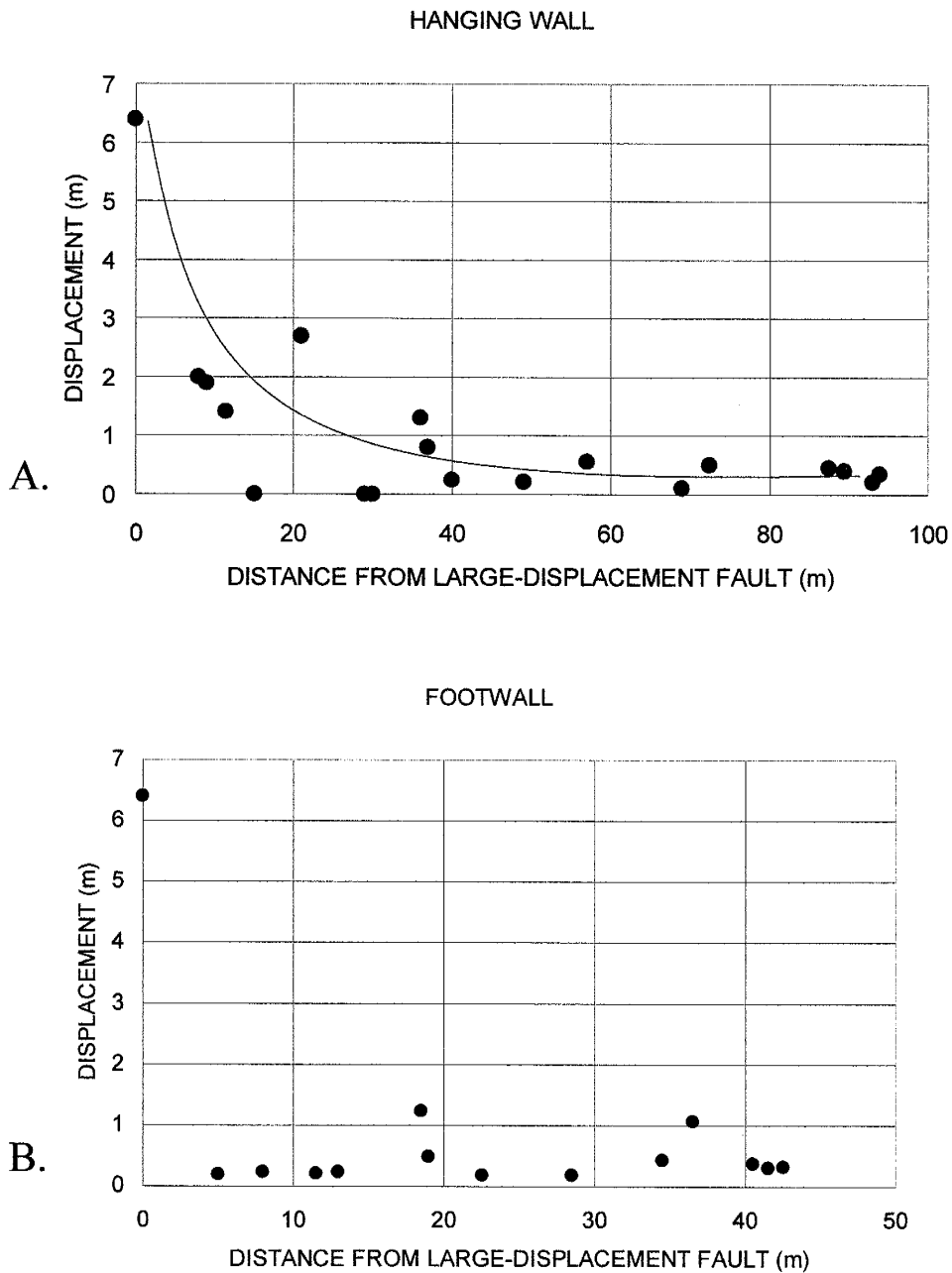


Figure 6: Plot of fault displacement versus distance from large-displacement fault for hanging wall (A) and footwall (B). Large-displacement fault is marked by the origin.



Figure 7: Photo of fault that cuts conglomerate at Canyon Trail site; fault zone is outline by yellow dotted lines. Note the smaller, more uniform grain size within the fault relative to the protolith and the absence of open fractures and slip surfaces.

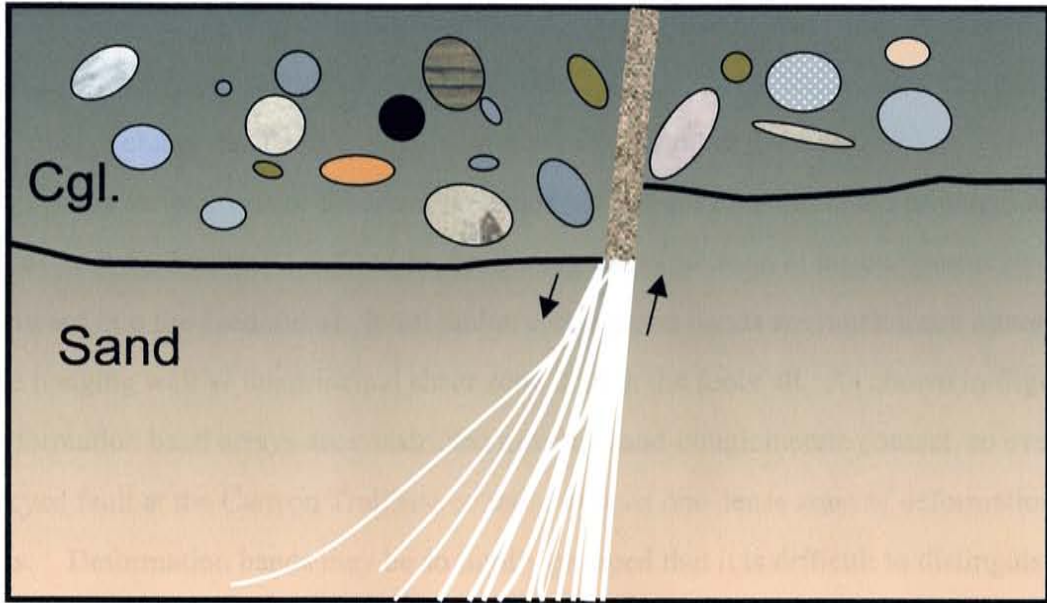


Figure 8: Schematic illustration showing how fault zone width increases downdip of conglomerate/sand contact. Note that distal deformation bands in the hanging wall have shallower dips.

weathered surfaces (Figure 9). They appear lighter in color than the host sand, but when wet they appear darker due to greater moisture retention (Figure 10). Cohesion of deformation bands is reduced when wet.

Nearly all deformation bands at the Canyon Trail Site are associated with a fault; few are solitary. Deformation band arrays at Canyon Trail are quite varied in their geometry. The sketch panels in Figure 11 show four end-member geometries: a single en echelon deformation band array, diffuse zones of largely subparallel deformation bands, dense zones of subparallel or anastomosing deformation bands, and complex synthetic-antithetic networks, or ladder structures (cf. Davis, 1999). Most faults at the Canyon Trail site are characterized by a mixture of these end-member geometries.

Most dense zones of deformation bands in sand are found near the principal shear zone of each fault (which I defined by continuing the shear zone in the conglomerate downward into the sand units). In all faults, deformation bands are much more numerous in the hanging wall of the principal shear zone than in the footwall. As shown in Figure 8, deformation band arrays are constricted near the sand-conglomerate contact, so every surveyed fault at the Canyon Trail site contains at least one dense zone of deformation bands. Deformation bands may be so tightly grouped that it is difficult to distinguish each band's boundaries (Figure 12). In less dense zones, deformation bands commonly appear to have an anastomosing geometry.

Solitary deformation bands associated with faults are typically observed in the footwall or at the distal edges of the array in the hanging wall. Typically, the deformation bands farthest from the principal shear zone are the most difficult to see and have the smallest displacements. Upon close inspection one sees that some bands are actually composed of multiple en echelon segments (Fig. 11a). Linkage of these overlapping segments creates "eye structures" similar to those seen in sandstone (e.g., Antonellini and Aydin, 1995). Riedel shears – conjugate shear geometries commonly observed in the field and laboratory (Riedel, 1929) – are apparent in many fault zones at Canyon Trail. For instance, the drawings show many deformation band segments whose dip angle is

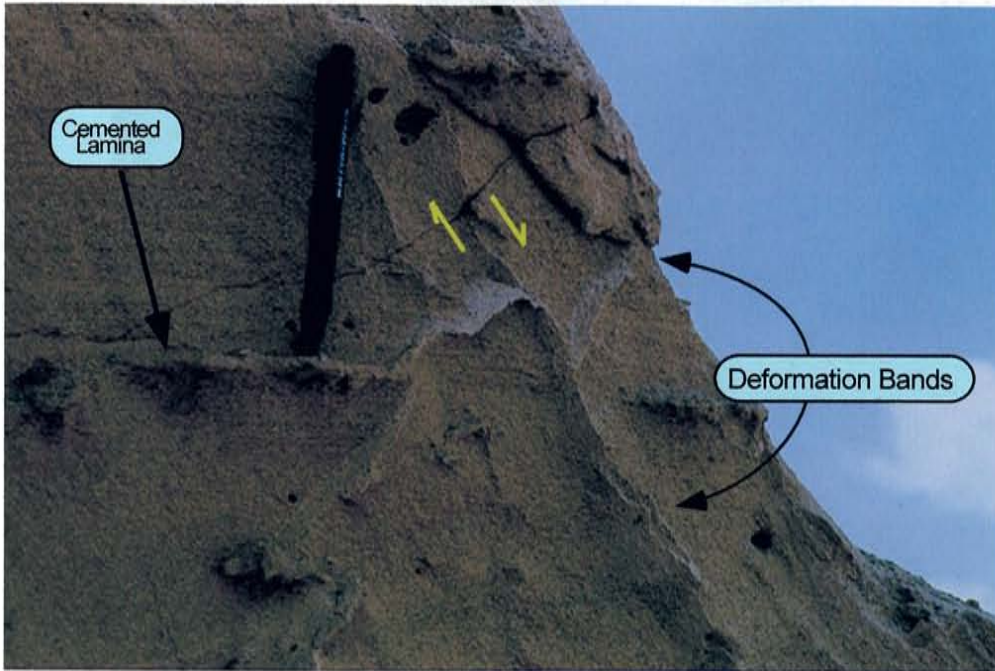


Figure 9: Two deformation bands showing cross-cutting relationship and displacements <10 cm. Deformation bands are resistant to weathering.

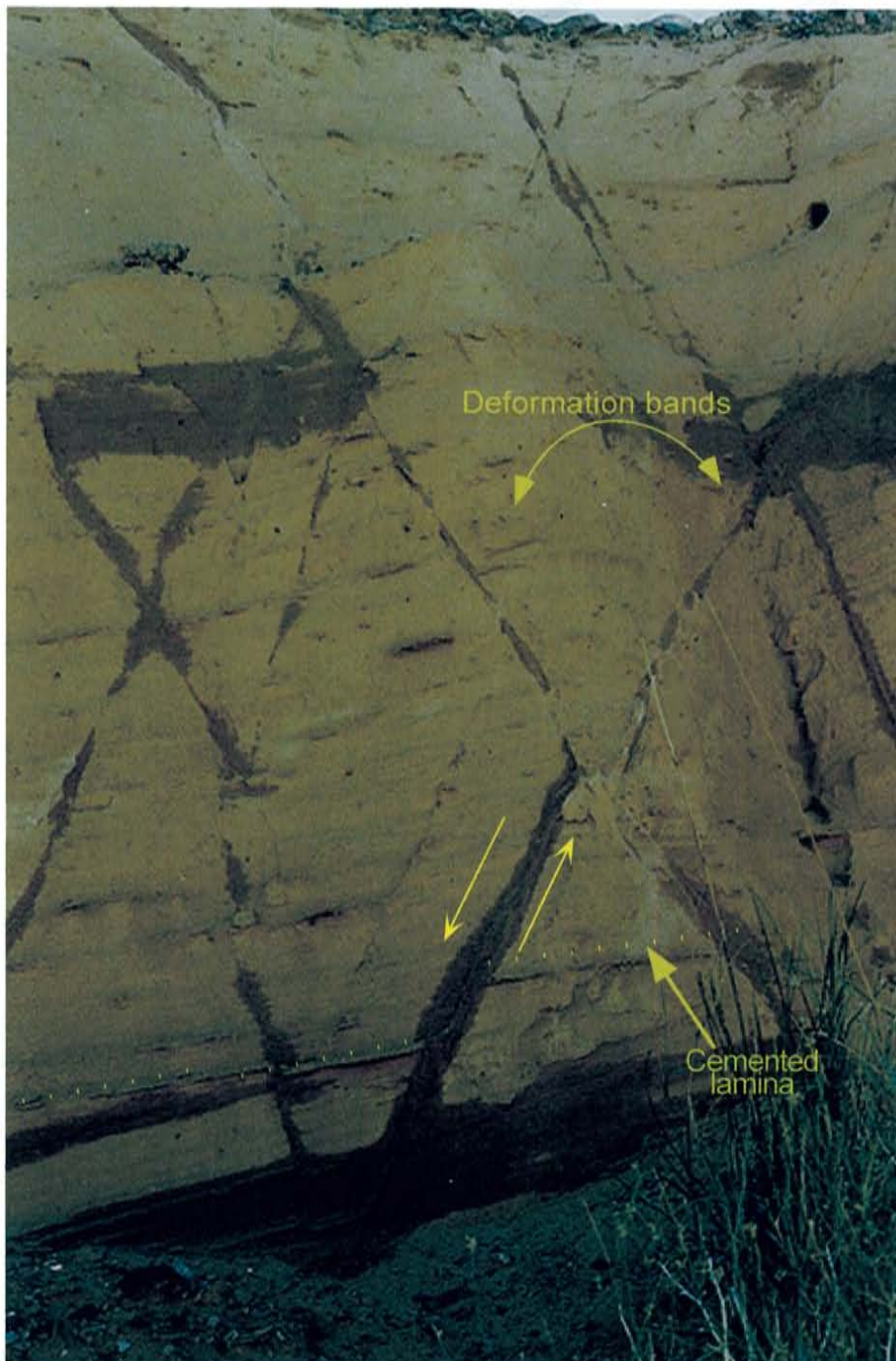


Figure 10: Photo of several conjugate deformation band sets cutting sand. Note the small magnitude of displacement (shown by highlighted cemented laminae) and the preferential wetting of the faults (dark, stained areas.) View is to the east of a north-striking outcrop face. Height of outcrop is approximately 4 meters.

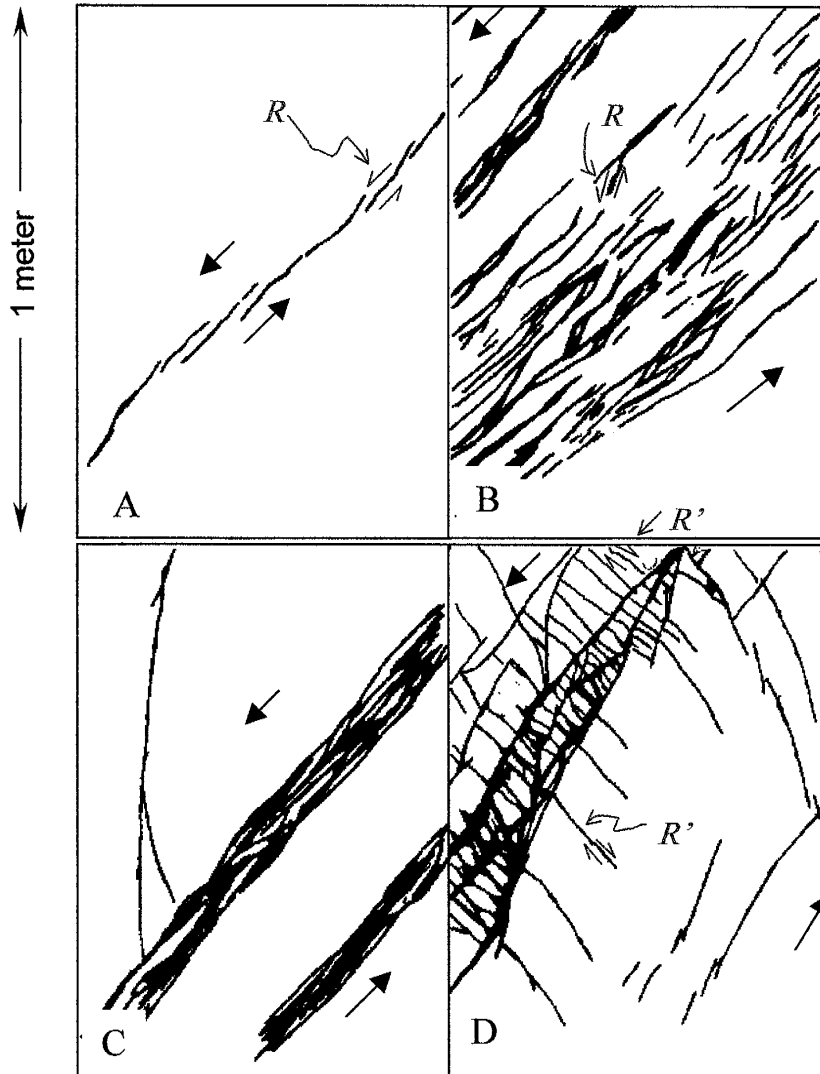


Figure 11: Detailed outcrop sketches showing the diversity of deformation band array geometry.

A: Individual deformation band segments. Note synthetic Riedel shears (R) and overlap of segment tips.

B: Diffuse zone of subparallel deformation bands with some local Riedel elements.

C: Narrow zones of anastomosing deformation bands.

D: Complex ladder structure created by deformation bands of opposing orientation and shear sense (R' shears).

Fault zone shear sense is down to the left in all examples, as shown by black arrows.

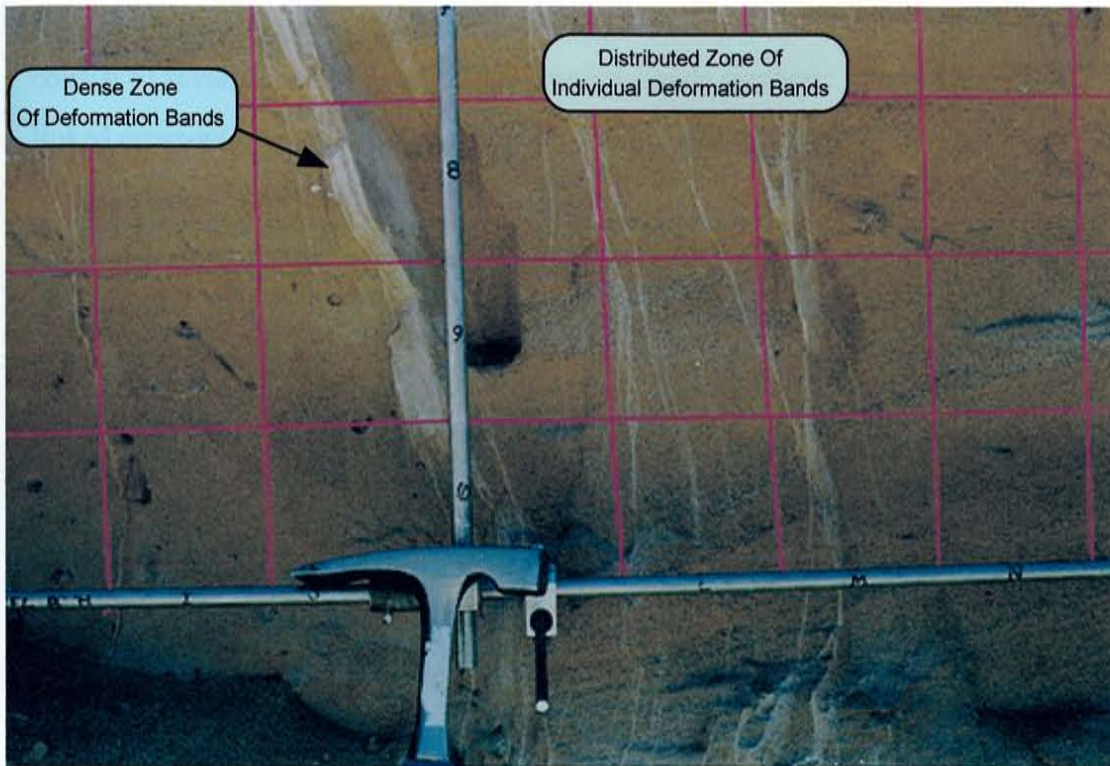


Figure 12: Photo showing occurrence of deformation bands both as individual bands distributed over a zone tens of centimeters wide, and as 1-3 cm zones of very closely spaced bands. View is to the east. Slip sense is down to the right. String grid is marked at 10 cm intervals.

slightly steeper than that of the main shear plane, which have a shear sense similar, or synthetic to, the main fault zone. Other segments have a dip sense opposing the main shear plane and a shear sense opposite, or antithetic to, the main fault zone. These correspond to R and R' Riedel orientations, respectively.

There are only a few well developed ladder structures at the study site, all associated with faults having displacements greater than 1 meter. Ladder structures consist of several narrow zones of deformation bands synthetic to the principal shear zone linked cross-wise by deformation bands of opposite dip sense (R' shears; Figure 11d). Crosscutting relationships show that these deformation bands of opposing dip have an antithetic slip sense. In some places synthetic bands cut antithetic bands, and in other places the opposite is true, suggesting both sets developed at approximately the same time. Lines formed by the intersection of these two sets are perpendicular to the grain lineations, which is the expected orientation if the lineations record the slip direction. Synthetic deformation bands in ladder structures have principal shear and Riedel R shear geometries, and the antithetic “rungs” have an R' orientation.

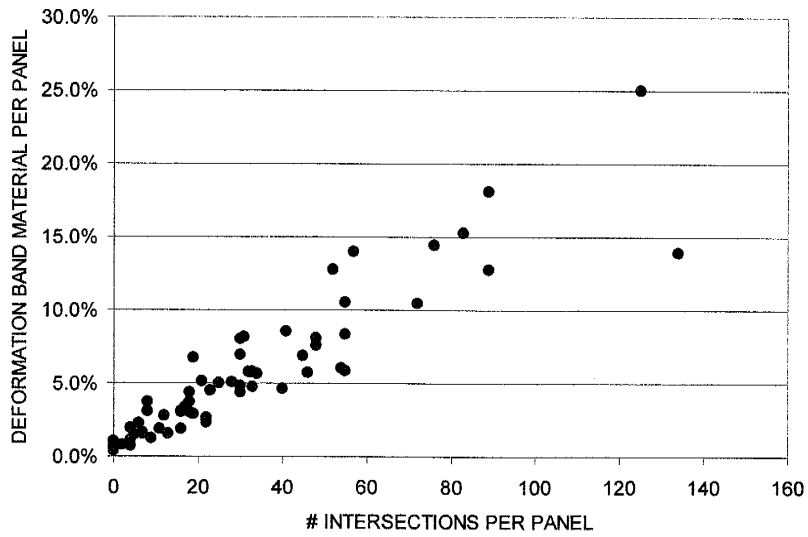
Digital images of the 1:10 outcrop maps (Appendix B) were processed to quantify certain deformation band array properties in order to evaluate relationships between deformation band array geometry and factors such as fault displacement or distance of the array from the large-displacement fault. These data indicate that the number of intersections increases with an increase in number of deformation bands (indicated by amount of deformation band material, Figure 13a). Surprisingly, however, the amount of deformation band material per fault does not increase proportionally with respect to displacement, as previously mentioned strain hardening models would suggest (Figure 13b). For example, one fault recording 40 cm of displacement shows 11% cross-sectional deformation band area, whereas one of 130 cm displacement shows only 5% deformation band area. Consideration of width versus displacement of narrow zones of deformation bands also shows no evidence for a direct relationship between the two, as observed in faults which cut sandstone. One such zone at fault E10 (Figure 12) has an average width

of 1 cm and an estimated displacement of 55 cm. Petrographic studies failed to distinguish individual deformation bands within this zone. Assuming a 1.5 mm width for each individual deformation band (a reasonable estimate based on my petrographic observations of individual deformation bands), the narrow zone of deformation bands at fault E10 could be composed of 6 or 7 adjacent deformation bands. If movement on each deformation band was arrested after 5 cm of slip, total displacement across this dense zone should be limited to approximately 30 cm – not 55 cm as indicated by the displaced strata. The chosen measure of deformation band array complexity, number of intersections per length of deformation band, also does not seem to be related to magnitude of fault displacement, and the percentage of deformation band material per fault does not appear to depend on distance from the large-displacement fault (Figure 14).

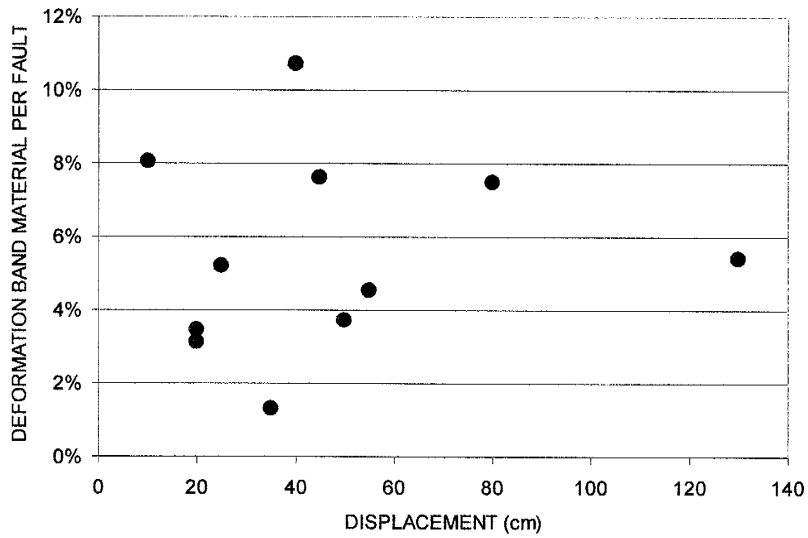
The relative proportion of north- and south-dipping deformation bands within each sketch panel varies with proximity to the large-displacement fault. Figure 15 shows that at distances greater than 50 m from the large-displacement fault, deformation band arrays are generally composed wholly of south-dipping deformation bands. Nearer the large-displacement fault, deformation band arrays are composed of a more even mixture of north- and south-dipping deformation bands. This is consistent with the earlier observation that conjugate fault sets are more common in proximity to the large-displacement fault (Figure 5).

Petrographic Observations

Twenty-one thin sections were made from hand samples of deformation bands in sand. Six of these thin sections were selected for point count analysis (Appendix A). Each of these thin sections contains at least one deformation band; one section (SH2) contains a narrow zone of deformation bands. Even though these samples came from several locations within the outcrop, the composition of the undeformed sand or parent material is remarkably uniform among all thin sections (Table 1). In most samples examined, the feldspar plus lithic fraction makes up one-third of the framework grain



A.



B.

Figure 13:

- a) Plot of number of deformation band intersections versus percentage of deformation band material per fault panel.
- b) Plot of deformation band material per fault versus fault displacement.

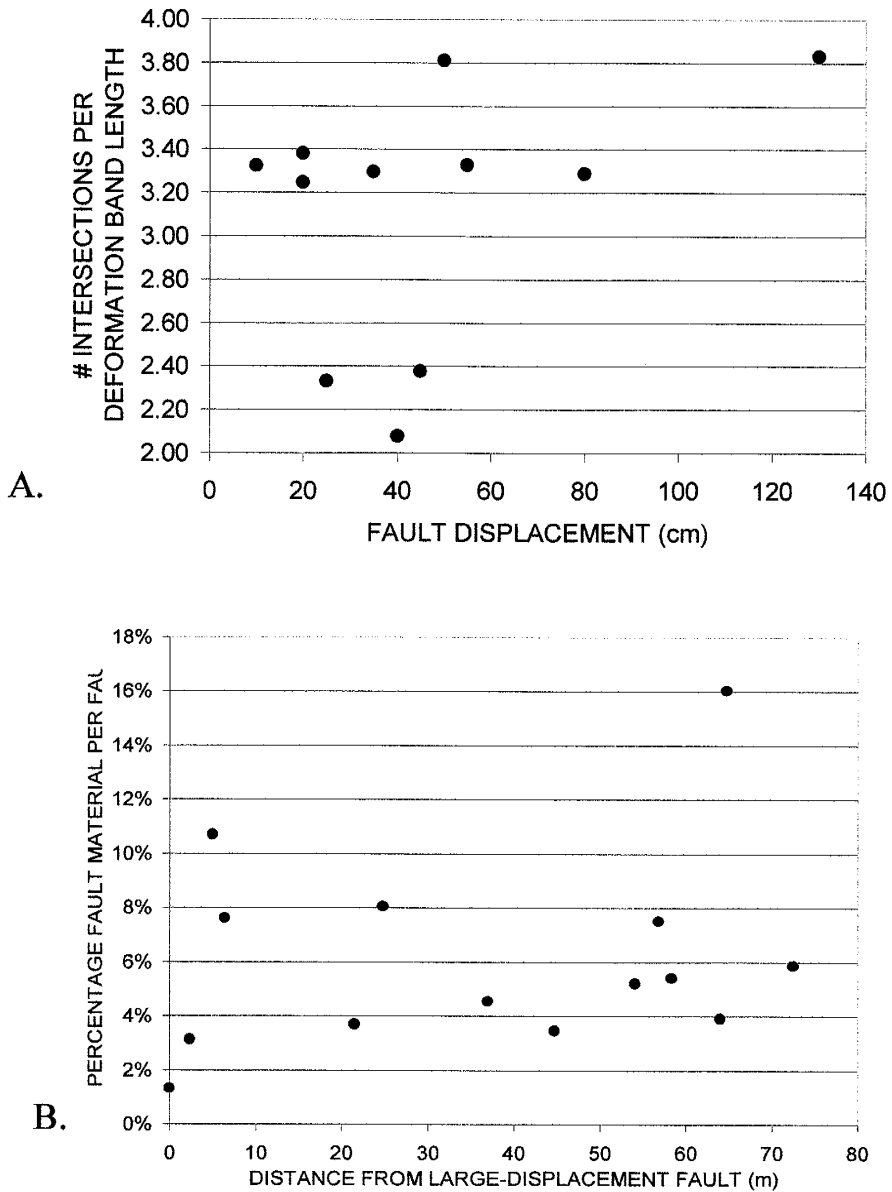


Figure 14:

a) Deformation band complexity index versus fault displacement.

b) Percentage deformation band material versus distance from large-displacement fault.

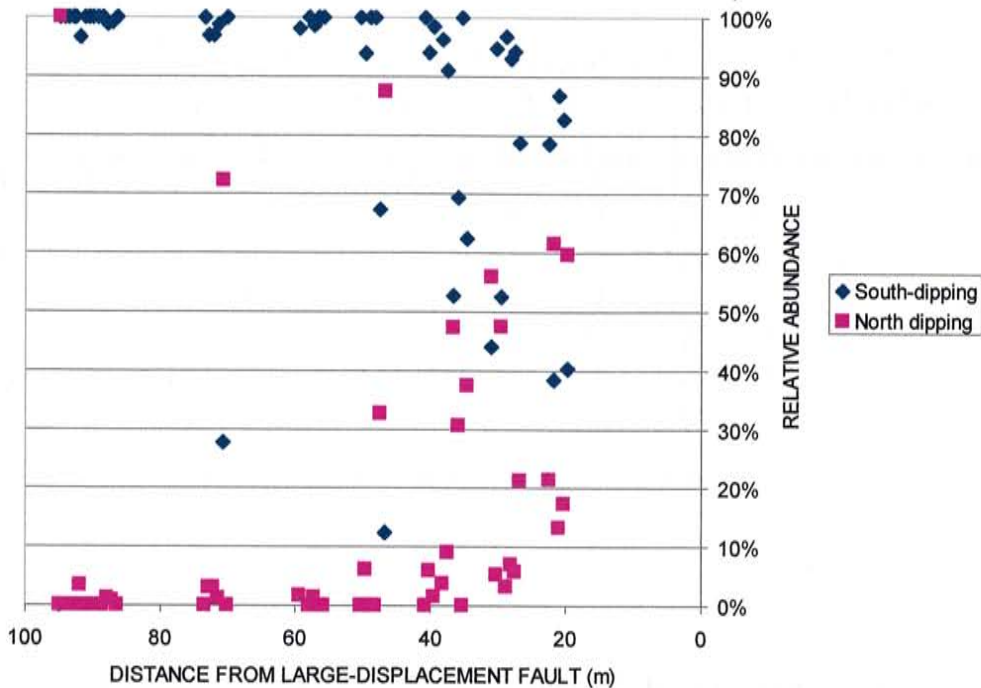


Figure 15: Distribution of north- and south-dipping deformation bands plotted against distance from large-displacement fault. Each 1:10 sketch panel is represented by one pink square and one blue diamond, representing the percentage of deformation bands within that sketch panel that dip to the north and south, respectively. It was not possible to make detailed deformation band maps adjacent to the large-displacement fault due to regolith cover and cavitation of the outcrop.

Table 1: Point count data. See text for definition of pseudomatrix and distinction between macroporosity and microporosity. **U** = undeformed parent sediment. **D** = deformation band material. 300 points were counted in the undeformed region of each thin section, and 150 points in the deformation band material of each thin section. Thin section **SH-2** contained too little undeformed sediment to obtain compositional data. See Appendix A for location and details of samples used for point counts.

	Sample ID										
	E-1		W-2		W-1		SH-1		TS 517993		SH-2
	U	D	U	D	U	D	U	D	U	D	D
Macroporosity	29	4	29	11	33	3	33	6	31	8	0
Microporosity	11	21	6	12	7	21	4	16	5	19	3
Quartz	18	29	19	30	17	29	18	23	19	25	31
Feldspar (sum)	16	6	12	10	12	11	10	8	10	10	16
Lithics	20	9	24	19	22	7	27	21	25	15	19
Pseudomatrix	4	27	5	13	4	27	4	25	5	20	30
Calcite	1	3	2	5	2	1	2	0	2	3	1
Other	1	2	4	1	2	1	2	1	3	1	1

composition. Due to the uncertainty in distinguishing feldspar type of very small grains, potassium and plagioclase feldspars were lumped together. The abundance of zoned plagioclase and volcanic lithic fragments suggests source areas rich in volcanic rock types, consistent with the observation that the conglomerates are rich in volcanic clasts. Rounded quartz overgrowths (recycled) are present on many of the quartz grains, and patches of microcrystalline calcite bridge some grains, but the samples studied were largely devoid of cements.

Point-count data collected from within each deformation band show a dramatic decrease in macroporosity and increase in fine-grained matrix relative to undeformed sand (Table 1). Macroporosity is reduced by a factor of five and is balanced by a commensurate increase in very fine-grained, brown, silt-sized matrix material. In plane-polarized light, deformation bands appear darker than the surrounding undeformed sand due to the lower porosity and abundance of this fine-grained matrix (Figure 16). Within

deformation bands, lithic and feldspar proportions are significantly reduced whereas quartz content is effectively increased relative to undeformed sand. The effect of deformation band formation on intergranular space is seen more clearly by normalizing the point count data to relative abundance of macroporosity, microporosity, and fine-grained matrix (Figure 17). Even though the samples from which the thin sections were made represent several faults of varying displacement and location, microstructural and composition characteristics were quite similar among all deformation bands. The one exception is the sample of a narrow zone of deformation bands (SH-2), which shows an even greater reduction in macroporosity than individual deformation bands (Table 1; Figure 17). (Due to an insufficient amount of undeformed material within the thin section of sample SH-2, protolith composition was estimated by averaging the protolith composition obtained from the other thin sections.)

The boundaries between deformation bands and host sand are distinct and are defined by the considerable contrast in porosity. At this scale of observation, many of the volcanic lithic grains appear to have deformed ductilely, although some are fractured. Back-scattered electron (BSE) images show that what appeared to be ductile deformation among the lithic grains is microscopically brittle (Figure 18a). The fine-grained matrix which occludes so much of the pore space within deformation bands is revealed to be silt-sized, angular fragments of feldspar, quartz, and lithic grains (Figure 18b). Most of the silt-sized particles composing the fine-grained matrix appear light grey in these BSE images, indicating that they are derived from feldspar and lithic clasts rather than quartz. The rough margins of many quartz framework grains, and the rarity of darker grey fragments in the matrix, show that quartz has also been fractured, although to a lesser extent than feldspar and lithic grains. Rather than undergoing wholesale cataclasis as the feldspar and lithic grains do, quartz grains are deformed through the chipping of small fragments from grain margins (cf. Rawling and Goodwin, submitted). The brown silt-sized material is therefore pseudomatrix produced from the deformation of labile grains (cf. Dickinson, 1970), rather than cement precipitated from solution. The presence of

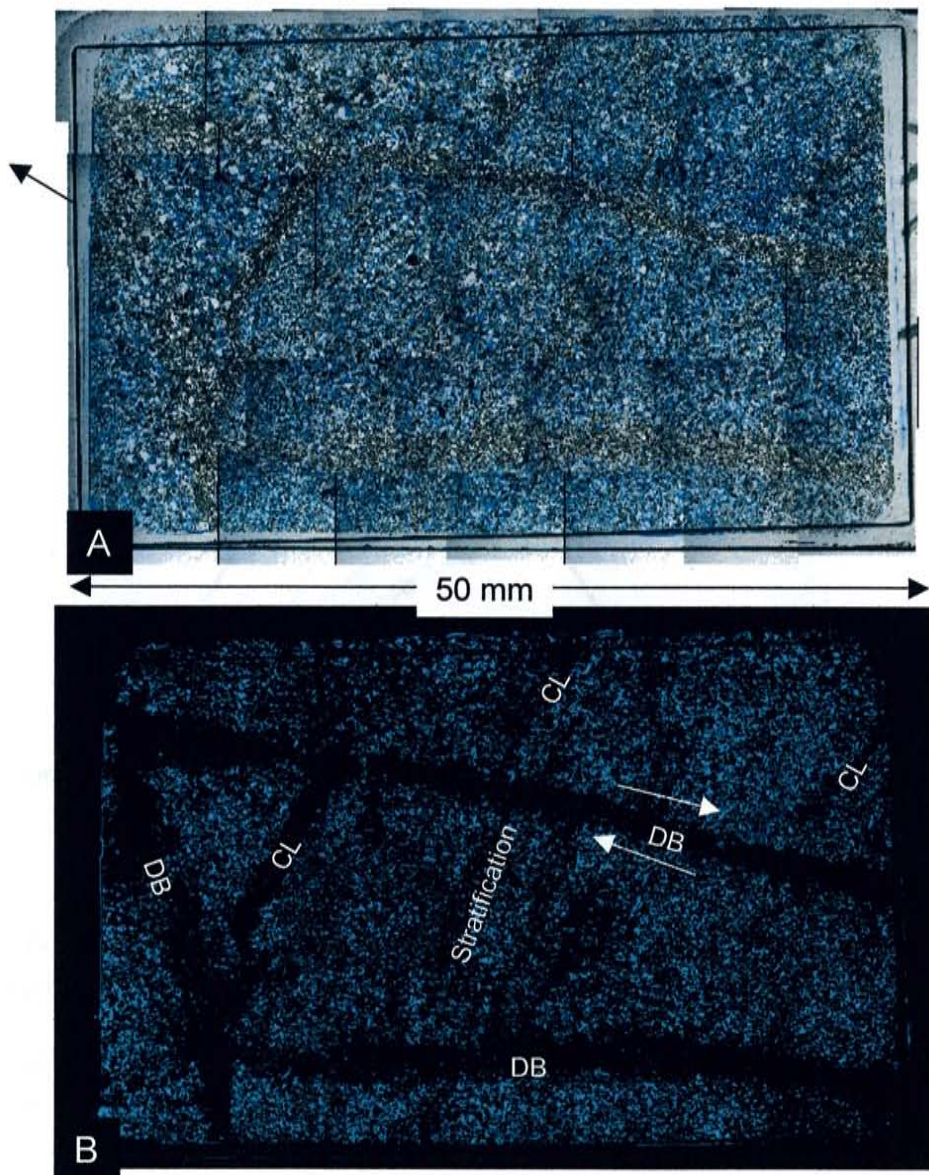


Figure 16:

a) Composite photomicrograph of a thin section (sample W-1) featuring a cross section of three deformation bands. Porosity appears blue due to dyed epoxy. Arrow shows stratigraphic way up.

b) Same thin section rendered in binary form to highlight structural and stratigraphic features. Pores appear blue, grains black. DB=deformation band, CL=clay lamina, arrows show shear sense on one deformation band.

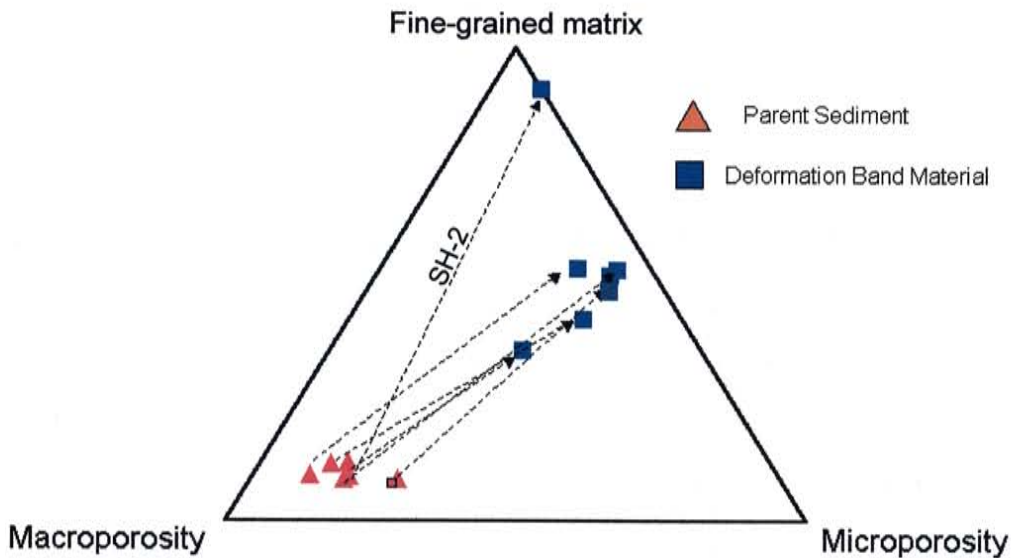


Figure 17: Ternary plot normalized to relative abundance of porosity and matrix. The intergranular space of undeformed parent sediment (red triangles) is dominated by large pores ($>0.5 \mu\text{m}$). During the development of a deformation band much of the macroporosity is destroyed, and intergranular space is dominated by fine-grained matrix and microporosity.

pseudomatrix in these deformation bands is not surprising given the relatively high percentage of volcanic lithic grains in the host sand, and the propensity of volcanic lithic grains to produce pseudomatrix (cf. Pittman and Larese, 1991).

Elemental X-ray maps revealed no difference in relative abundance of major elements between deformed and undeformed regions. False color images obtained by superposing selected elemental maps (e.g., silicon, aluminum, magnesium, potassium) were helpful in highlighting some microstructural characteristics and distinguishing between quartz and non-quartz grains. These images showed that the mean grain size of non-quartz constituents is less within the deformation band than without, whereas the size of quartz grains remains relatively constant in both regions. This agrees with point count results which show an apparent enrichment of quartz within deformation bands (Table 1). Because quartz grains are not as severely diminished in size as feldspar and lithic grains within deformation bands, the ratio of identifiable quartz to non-quartz grains increases in favor of quartz. These observational data also agree with the petrographic and microstructural studies of other authors which show quartz to be mechanically stronger than feldspar and lithic grains under the low temperature and pressure conditions at which these sediments were probably deformed (e.g., Pittman and Larese, 1991; Swierczewska and Antoni, 1998).

In-place fractured feldspar, quartz, and accessory mineral grains are present in every thin section, both within and without deformation bands. Blue epoxy within grain fractures indicates the fractures were present when the sample was taken from the outcrop and are not a result of thin section preparation (Figure 19). Fractured grains appear to be more common in the less deformed parent material. This apparently counter-intuitive observation is probably due to the higher strains within deformation bands which distribute grain fragments over a larger area, thus making it more difficult to determine which fragments came from a single grain.

In most thin sections, stratification within the host sand can be observed by the preferred alignment of elongate grains parallel to bedding. Within deformation bands,

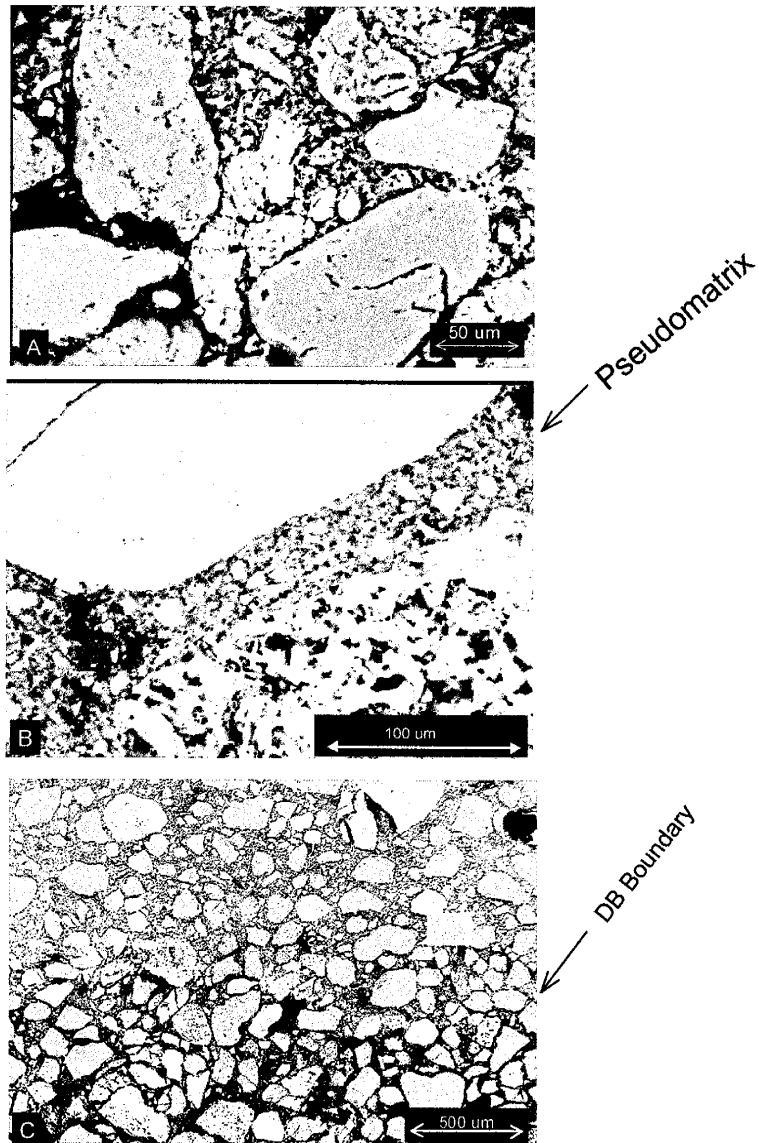


Figure 18: BSE images illustrating microstructures that record microscopically brittle deformation mechanisms. Grey levels in these images reflect average atomic number (Z) of sample; brightness increases with Z -number. Quartz (Q) therefore appears grey, feldspars (F) and lithic fragments (L) are a lighter grey. Pores (epoxy) appear black. All images are from sample SH-2.

A: Lithic grain (L) impinged upon by stronger quartz (Q) grains, showing numerous microfractures.

B: Higher magnification view resolving matrix material as angular, silt-sized feldspar, lithic, and quartz fragments.

C: Relatively low magnification view of boundary between deformation band (DB) and relatively undisturbed sediment. Note the low porosity, dominance of quartz sand grains, and large percentage of pore-filling pseudomatrix in the deformation band.

many elongate grains are aligned subparallel to the dip of the band. In the area immediately adjacent to deformation bands, elongate grains have been rotated to an orientation intermediate between that of the deformation band and that of the undeformed sand. Qualitative and quantitative measurements confirm these observations (Figure 20).

While nearly all the deformation bands at the Canyon Trail site are not cemented, it should be noted that these would seem to be favorable locations for cement growth. As more grain surface area is exposed through cataclasis, and as the distance between grains decreases it becomes easier to nucleate cements. In fact, Berner (1980) notes that it is theoretically possible to nucleate cements from an undersaturated solution. Just a few hundred meters south of the Canyon Trail site is a location where all of the deformation bands have been preferentially cemented, while the surrounding undeformed sand is still largely unlithified.

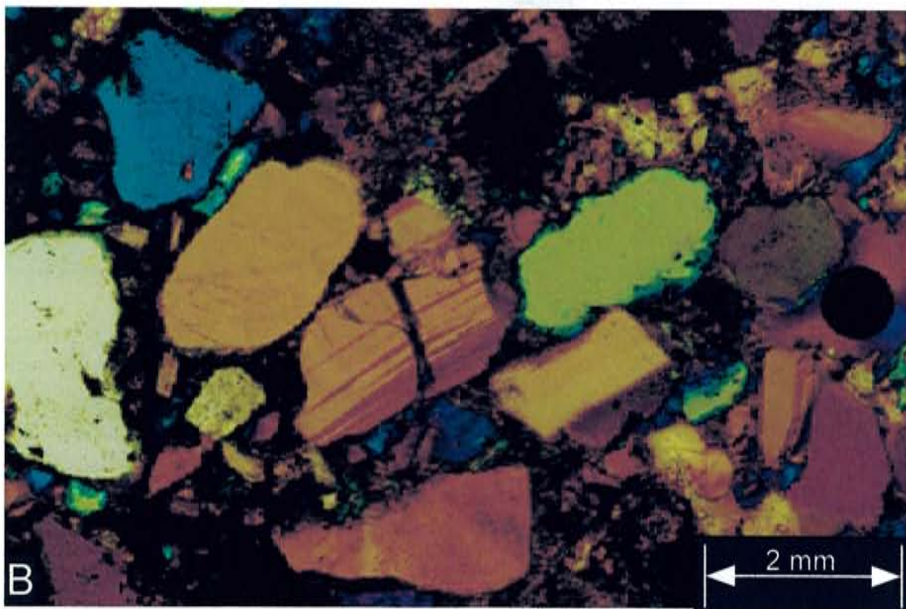
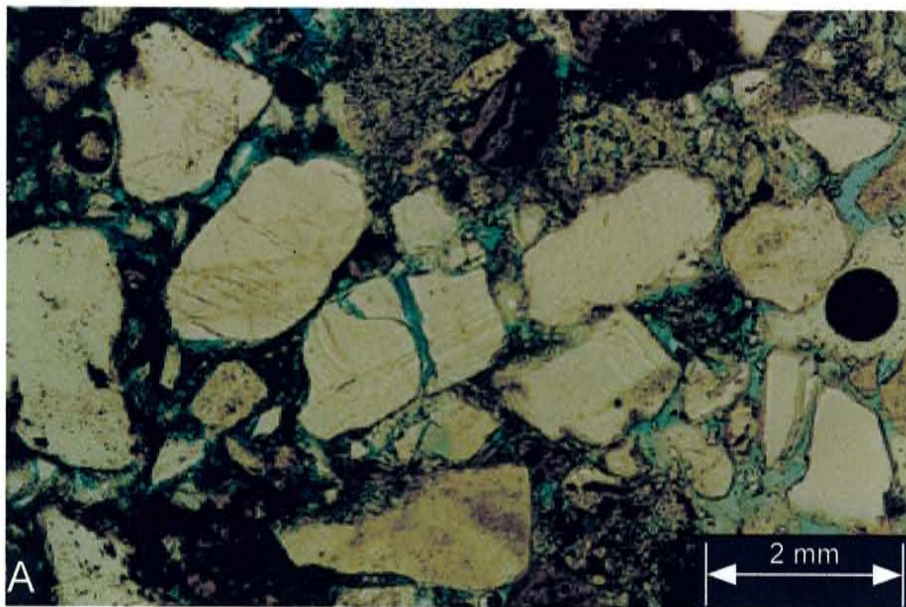


Figure 19: Photomicrograph in plane polarized (A) and cross polarized light with gypsum plate inserted (B) showing fractured grains near deformation band. Note in-place fractured feldspar grain at center.

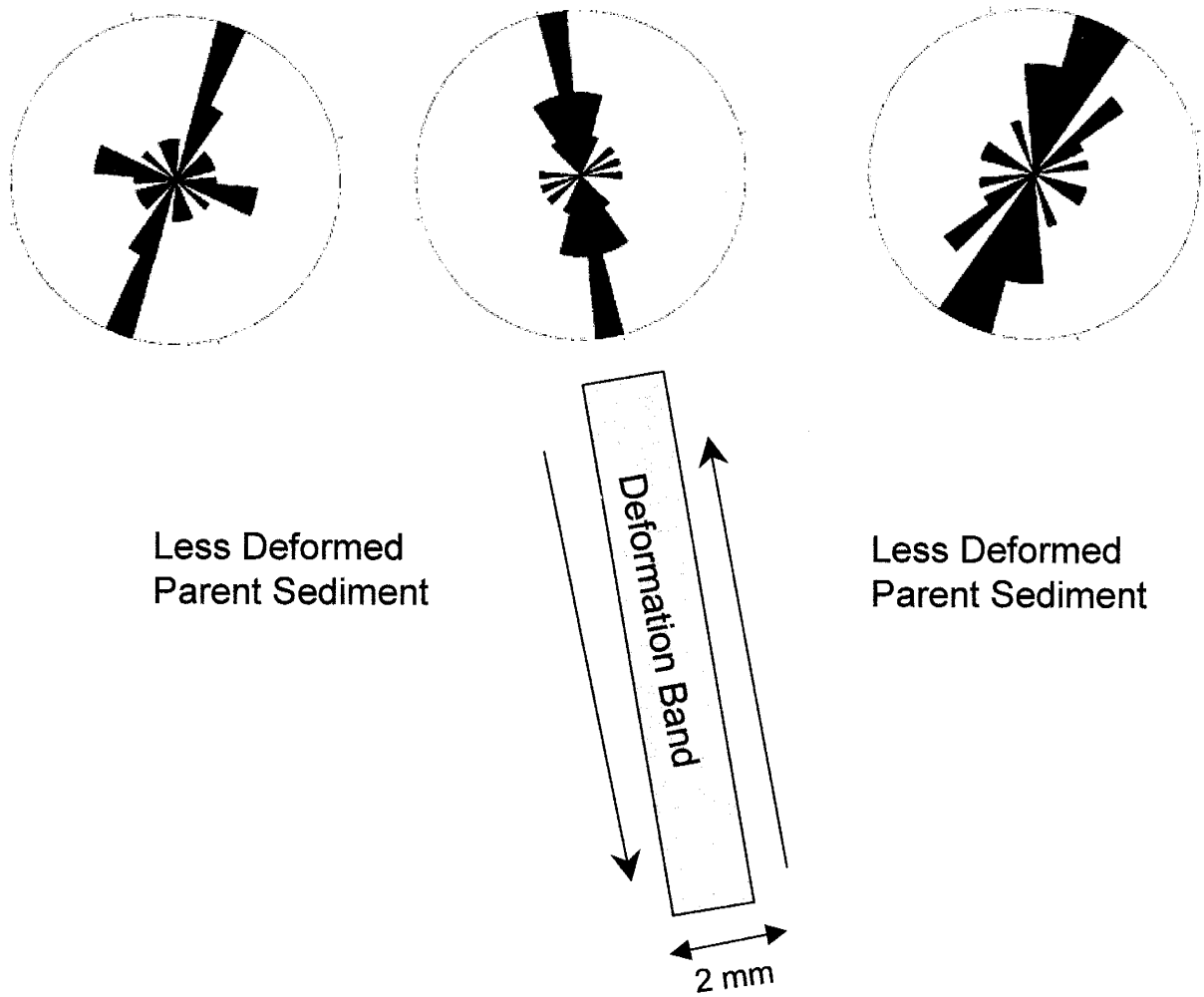


Figure 20: Rose diagrams at top show preferred orientation of grains within deformation band (center) and on either side of deformation band. Elongate grains within deformation bands have been rotated into the plane of the band. Sample was collected near surveyed fault W5. A total of 109 points were counted.

DISCUSSION

Age and Character of Faulting

The NW-SE orientation of all faults at the Canyon Trail site, and the fact that all show normal dip-slip displacement, agrees with the overall NE-SW extension of this portion of the Rio Grande Rift (Chapin and Cather, 1994). It is difficult to determine the age of these faults. Certainly they are at least as young as the Oligocene-Miocene sediments they cut, and probably younger as no evidence was found for syn-tectonic sedimentation. Continuing seismic activity in the area has produced Holocene fault scarps (Machette, 1982), but the absence of any post-Popatosa sediments at the Canyon Trail makes it difficult to better constrain fault ages. It is interesting to note that almost all faults south of the large-displacement fault (hanging wall) dip to the southwest, whereas on the north side (footwall) conjugate sets of northeast- and southwest-dipping faults are common (Figure 5). This may indicate a pure shear deformation style in the footwall, with horizontal extension and vertical shortening, and a simple shear or rotational deformation style in the hanging wall. In any case, the hanging wall appears to be accommodating more extension than the footwall.

Development of Deformation Band Arrays

Figure 2 indicates that one of the key elements in applied fault/fluid flow studies is understanding the geometry, structural make-up, and petrophysical properties of each fault zone. Knowing which features to expect with a fault of a given displacement or distance from a large-displacement fault would be a very powerful predictive tool in aquifer or reservoir flow simulations. In applying such a tool, however, the worker should be careful to draw on apposite studies for the reservoir or aquifer in question. For

instance, a conceptual model of fault-zone architecture and permeability structure developed from studies in crystalline rocks may not be applicable to a reservoir of porous sandstone. The deformation band arrays at the Canyon Trail site appear at first to be identical to deformation band arrays in sandstone, but closer examination of the outcrop, petrographic, and microprobe data yields important differences. Thus, previous deformation band models (e.g., Aydin and Johnson, 1978) probably should not be used to predict the characteristics of fault zones which cut poorly lithified lithic-rich sand.

The first, obvious observation that the faults at the study site are expressed as zones of cataclastic deformation bands rather than discrete slip surfaces, is an important one. As mentioned previously, many high porosity sandstones also deform by formation of deformation bands rather than fractures or slip surfaces. In addressing the failure behavior of sandstones, Wong et al. (1997) conclude that the transition from brittle, localized shearing to cataclastic flow depends largely on porosity and grain size. For a given effective pressure, low porosity and small grain size favor the formation of fractures whereas high porosity and large grain size favor cataclastic flow. Holding porosity and grain size constant, cataclastic flow is more likely to occur at higher confining stresses. The basic mechanics of these two failure behaviors are the same – grain-scale microcracking – but whereas shear localization arises from coalescence of microfractures, cataclastic flow develops from distributed microfracturing (Menendez et al, 1996). The porosity and grain size of the Canyon Trail sands are comparable to sandstones in which deformation bands are common, and with no cement to inhibit grain-scale mixing, it would be very difficult for transgranular microfractures to coalesce into a through-going slip surface. Thus it seems that for sands with porosities and grain sizes similar to those at the study site, zones of deformation bands would be the primary means of accommodating moderate fault displacement.

It is also desirable to know how a zone of deformation bands grows with increasing displacement. Do these deformation band arrays develop through a systematic addition of deformation bands with increasing displacement? Most field studies of

deformation bands since Aydin and Johnson (1978) conclude that zones of deformation bands do grow systematically through the addition of one band after another. After the first deformation band is formed, porosity collapse and shear-enhanced compaction lead to strain-hardening, inhibiting shear localization. As a result a new deformation band forms adjacent to the first, and the first accommodates no further displacement. The faults at the Canyon Trail site, however, do not exhibit a relationship between magnitude of fault displacement and number of deformation bands (Figure 13b). To account for this lack of correlation, one would suppose that certain deformation bands or zones of deformation bands probably remained active or were reactivated as deformation continued. Petrographic evidence lends support to this hypothesis. The dense zone of deformation bands at fault E10 (Figure 12) shows much lower deformation band porosity relative to other deformation bands in this study. If we assume that the greater loss in porosity (and greater relative abundance of matrix material) is caused by greater deformation, then this observation supports the outcrop observations that zones of deformation bands cutting partially lithified sand may not exhibit a linear relationship between displacement and number of deformation bands as seen in their sandstone counterparts.

In spite of this difference in strain-hardening behavior, as well as differences in mineralogy and degree of induration or cementation, it is somewhat surprising to see so many similarities in the outcrop expression of deformation band arrays in quartz arenites and the poorly lithified Popatosa sand. Both project in positive relief from weathered surfaces. Davis (1999) notes that resistance to weathering is aided by pore collapse and preferred cementation within the band, but most of the deformation bands at Canyon Trail contain little, if any, cement (Table 1). Instead, the pseudomatrix apparently acts as a weak mortar. As mentioned earlier, many geometric characteristics of deformation band arrays, such as eye structures and ladder structures, are common to deformation bands which cut quartz arenites and those which cut unlithified sand. Do the arrays at the Canyon Trail site develop in the same manner as those in sandstone? My outcrop

sketches of complex structures, like ladder structures, closely match the geometry of ladder structures found in sandstones (Davis, 1999). After studying ladder structures in Navajo sandstone, Ahlgren (1999) proposed a process by which these distinctive and complex structures form. In his conceptual model, unconnected deformation band segments develop at a high angle (R' orientation) to the trend of the principal shear zone. Narrow, through-going zones of deformation bands synthetic to the principal shear zone cross cut these “external R' surfaces” and accommodate most of the strain. Finally, smaller “internal R' ” form and link the synthetic, through-going deformation bands. Crosscutting relationships at the Canyon Trail ladder structures support the kinematics of Ahlgren’s model. However, the hypothesis that R' surfaces were the first structures to form derives from observations of R' deformation bands extending beyond the main ladder structure (G. Davis, pers. comm., 2000). Due to limited exposures of ladder structure shear zones at the Canyon Trail site I was not able to confirm this observation. That deformation band arrays at the Canyon Trail site share so many geometric characteristics with deformation band arrays in sandstones suggests that lithification state may have little bearing on the formation of ramp, eye, and ladder structures. These forms of deformation band arrays may simply be recording the kinematics of normal faulting in sands and arenites.

Figure 13a shows a direct correlation between the percentage of deformation band material and the number of intersections per map panel. I interpret this as evidence that deformation bands tend to link with each other as the array grows. Even in distributed zones of subparallel deformation bands, as seen in Figure 11b, most bands intersect at least one other band. If an array grew through the addition of deformation bands, and each new band was exactly parallel to the previous one, we would not see the relationship implied by Figure 13a. I know of no study showing a similar relationship for deformation bands cutting sandstones, but given the similarities in array geometry I presume the same correlation holds. This observation may be significant when applied to studies of fluid flow at the outcrop scale. Lower porosity and smaller pore size within

deformation bands leads to a lower single-phase permeability, thus deformation bands would retard cross-fault fluid flow. In an array of linked deformation bands, such as the one pictured in Figure 14d, fluid flow would be retarded both normal to the shear zone and parallel to the shear zone dip. If the array were composed of a series of parallel deformation bands which were not linked, fluid flow might be relatively unimpeded parallel to the shear zone dip. The graph in Figure 16a indicates that we are safe in assuming deformation band arrays are composed of linked bands, and thus dip-parallel fluid flow will be impeded by deformation band obstructions or tortuous flow paths.

Despite the many similarities between deformation bands and deformation band arrays at Canyon Trail and those described in quartz arenites, there are also several differences to note. First, most deformation bands at my study site are concentrated in the hanging wall of each fault. Observations of faults cutting Entrada and Navajo sandstones indicate, in contrast, that most or all of the deformation bands in well lithified quartz arenites are located in the footwall (relative to the slip surface or principal shear zone; Aydin and Johnson, 1978). All deformation bands at my study site are at least 1.5 mm wide, which is a typical width for deformation bands in sandstone as well, but I have also observed much narrower bands – perhaps 0.5 mm wide – cutting sandstones at many locations throughout the Colorado Plateau, Basin and Range, and Rocky Mountain Front Range provinces. No such narrow deformation bands were observed at the Canyon Trail site. In sandstones I have often observed isolated deformation bands, or networks not associated with any nearby fault, but at the Canyon Trail site all deformation bands are linked to one of the 30+ surveyed faults.

Keeping these differences in mind could be useful when studying deformation bands in sandstones and trying to determine whether the bands were formed pre- or post-lithification. Some geologists have used the presence of cataclasis as a criterion for determining whether the deformation bands were formed in unlithified sand or sandstone (Antonellini et al., 1994). As we see in the photomicrographs and BSE images from the Canyon Trail samples, however, cataclasis also occurs in poorly lithified sand. Whether

the spatial density of deformation bands is higher in the footwall versus the hanging wall seems to be a better indicator of lithification state. For instance, if one encountered a fault zone in which most of the deformation bands were concentrated in the hanging wall, one could suppose that this zone formed before the sand had become cemented. Other characteristics which seem to be unique to deformation bands cutting sandstones may also be used to infer lithification state at the time of deformation, such as if one encountered a single, lone deformation band of very narrow (0.5 mm) width.

Compositional Controls on Deformation

The previous section compared and contrasted deformation band arrays in sandstone versus partially lithified sand. What is different about deformation of Entrada Formation quartz arenites and deformed Santa Fe Group sand? Conditions of deformation, such as stress state, magnitude and number of slip events, are not well constrained at the Canyon Trail site. We can, however, say that important differences exist between the lithologic characteristics of Santa Fe Group sand and the quartz arenites which were the subject of many of the studies cited in the Previous Studies section. Whereas a sandstone such as the Entrada may contain 90% quartz and be well indurated, the sands at the Canyon Trail site are not well cemented and contain a large proportion of feldspar grains and lithic fragments (Table 1). It is important to note this abundance since lithic grains, particularly volcanic rock fragments, deform more readily than quartz or feldspar (Pittman and Larese, 1991). This is shown in my BSE images and petrographic point count data (Figures 17 and 20). The BSE images show that the pseudomatrix is largely composed of fine, angular fragments of feldspar and lithic grains, with a relatively small proportion of quartz particles. BSE images and photomicrographs from this and related studies on similar sediment show that feldspar and lithic grains that experienced brittle deformation at relatively low confining stresses deformed by wholesale comminution, whereas quartz grains tend to lose mass through the flaking off of small particles around the grain margins (Marone and Scholz, 1989; Rawling and Goodwin,

submitted). These observations raise the question of whether cataclastic deformation bands occur in “clean” nearly pure quartz unlithified sand. Given that silt-sized quartz fragments make up a relatively small proportion of the pore-occluding matrix material (based on my BSE observations), it would be interesting to know whether deformation bands in unlithified quartz sands are capable of reducing porosity and permeability as much as those at the Canyon Trail site.

Where they cut the conglomerate units the faults, as noted, are characterized by a shear zone, recessive in profile, relatively narrow (as compared to the same fault in the sand units), the width of which remains fairly constant along strike and dip. The most obvious lithologic differences between the sand and conglomerate units at this site are the degree of sorting and degree of induration. Since no samples of the conglomerate were processed for microscopic imaging, we don’t know anything about the deformation microstructures in this rock which might help us understand its deformation behavior. It is clear, though, that the processes responsible for fault zone widening in the sand, through the creation of new deformation bands, are not operating in the conglomerate to the same extent. During the early stages of faulting, the principal fault plane may have been a location where fine-grained sand and small pebbles were sifted from the poorly sorted mixture of sand, cobbles, and boulders. Accommodating additional strain was apparently easier in this fine-grained zone, and as faulting progressed, deformation was restricted to this narrow zone of finer grained sediments rather than branching outward as happened in the better sorted sand units.

CONCLUSIONS

Small-displacement normal faults (displacement <3 m) are expressed as arrays of deformation bands where they cut partially lithified sand, and as shear zones where they cut conglomerate. Nearly all small-displacement faults in the hanging wall, relative to a moderate-displacement fault, are synthetic to the moderate-displacement normal fault, whereas conjugate fault sets are common in the footwall. Similarly, within each small-displacement fault zone, most deformation bands in the hanging wall agree in dip direction and magnitude with the that of the principal shear zone, whereas the footwall is typically characterized by antithetic and synthetic arrangements of deformation bands. In the hanging wall of the moderate-displacement fault, small fault displacement increases with proximity to the moderate-displacement fault, but in the footwall no such relationship exists.

The width of the fault zones is fairly constant where the faults cut conglomerate units, but varies where they cut sand. Deformation band arrays are most narrow where they intersect the sand-conglomerate contact and generally widen downdip from this point. No relationship could be found relating the width of the array to distance from the moderate-displacement fault or total displacement. Array complexity seems to be only slightly related to total displacement, in that the most complex deformation band arrays (ladder structures) are only found associated with faults having total displacements greater than 1 meter. Within each deformation band array, the ratio of antithetic to synthetic band orientations increases with decreasing distance from the moderate displacement fault.

In terms of general outcrop appearance and geometry, the deformation band arrays show characteristics similar to those which cut quartz arenites. Outcrop measurements,

petrographic studies, and electron microscopy of deformation bands which cut Santa Fe Group sands, however, yielded two important differences: 1) most deformation bands occur in the hanging wall of each fault, and 2) there is no linear relationship between fault displacement and the number of deformation bands in a fault zone.

This study provides unequivocal evidence that cataclasis does occur even in unlithified, shallowly buried sediments. Feldspar grains and lithic fragments are most susceptible to fracturing, and quartz deformation is largely limited to grain margins. The commonly held notion that lithification and high confining stresses are prerequisite for cataclasis clearly can no longer be used to infer the timing and environment of deformation. That is, the presence of cataclastic textures in a rock does not explicitly indicate the rock was lithified and deeply buried at the time of deformation, as the deformation bands at the Canyon Trail site cut Tertiary sands which have very little cement and which have never been buried very deeply. This study suggests that better indicators of lithification state would utilize the relationships between fault density and location relative to the principal shear zone (footwall or hanging wall) and between total fault zone displacement and fault zone width.

Silty pseudomatrix generated by the comminution of feldspar and lithic fragments results in a five-fold decrease in porosity relative to the protolith as a result of cataclasis. With a reduction in porosity comes a reduction in permeability and, consequently, small faults which cut unlithified sand must not be ignored in groundwater studies, fault seal analyses, or petroleum reservoir evaluation. While few of the deformation bands at the Canyon Trail site were cemented, grain size reduction and pore collapse within deformation bands make these sites favorable for cement nucleation, thus preferential cementation of deformation bands may create even greater contrasts in porosity and permeability between the undeformed and deformed sand.

That the geometry and width of deformation band arrays which cut these Santa Fe Group sands cannot be predicted from fault displacement is also important. Since knowledge of the geometry and width of zones of deformation bands is such an integral

component of fluid flow modeling efforts, workers should take special care to account for fault-zone heterogeneity when dealing with aquifers and reservoirs composed of unlithified or partially lithified sand.

REFERENCES CITED

- Ahlgren, S., 1999, New interpretations of the sequential development of three dimensional deformation band shear zone networks in the Navajo Sandstone, Southern Utah: ABSTRACT: AAPG Bulletin, v. 83.
- Antonellini, M., and A. Aydin, 1994, Effect of faulting on fluid flow in porous sandstones: petrophysical properties: American Association of Petroleum Geologists Bulletin, v. 78, p. 355-377.
- Antonellini, M., and A. Aydin, 1995, Effect of faulting on fluid flow in porous sandstones: Geometry and spatial distribution: American Association of Petroleum Geologists Bulletin, v. 79, p. 642-671.
- Antonellini, M. A., A. Aydin, and D. D. Pollard, 1994, Microstructure of deformation bands in porous sandstones at Arches National Park, Grand County, Utah: Journal of Structural Geology, v. 16, p. 941-959.
- Aydin, A., 1978, Small faults formed as deformation bands in sandstone: Pure and Applied Geophysics, v. 116, p. 913-930.
- Aydin, A., and A. Johnson, 1978, Development of faults as zones of deformation bands and as slip surfaces in sandstone: Pure and Applied Geophysics, v. 116, p. 931-943.
- Berner, R. A., 1980, Early Diagenesis--A Theoretical Approach: Princeton, Princeton University Press, 241 p.
- Bouvier, J. D., K. Sijpesteijn, D. F. Kluesner, C. C. Onyejekwe, and R. C. Van der Pal, 1989, Three-dimensional seismic interpretation and fault sealing investigations, Nun River field, Nigeria: AAPG Bulletin, v. 73, p. 1397-1414.
- Burns, L. K., and F. G. Ethridge, 1977, Petrology and diagenetic effects of graywacke sandstones--Eocene Umpqua Formation, Southwest Oregon: ABSTRACT: American Association of Petroleum Geologists Bulletin, v. 61, p. 1374.

- Caine, J. S., J. P. Evans, and C. B. Forster, 1996, Fault zone architecture and permeability structure: *Geology*, v. 24, p. 1025-1028.
- Carter, K., and C. Winter, 1995, Fractal nature and scaling of normal faults in the Espanola Basin, Rio Grande Rift, New Mexico: implications for fault growth and brittle strain.: *Journal of Structural Geology*, v. 17, p. 863-873.
- Cashman, S., and K. Cashman, 2000, Cataclasis and deformation-band formation in unconsolidated marine terrace sand, Humboldt County, California: *Geology*, v. 28, p. 111-114.
- Cather, S. M., R. M. Chaberlin, C. E. Chapin, and W. C. McIntosh, 1994, Stratigraphic consequences of episodic extension in the Lemitar Mountains, central Rio Grande rift, in G. R. Keller, and S. M. Cather, eds., *Basins of the Rio Grande Rift: Structure, Stratigraphy, and Tectonic Setting*, Boulder, Colorado, Geological Society of America, p. 157-170.
- Chapin, C. E., and S. M. Cather, 1994, Tectonic setting of the axial basins of the northern and central Rio Grande rift, in G. R. Keller, and S. M. Cather, eds., *Basins of the Rio Grande Rift: Structure, Stratigraphy, and Tectonic Setting*, Boulder, Colorado, Geological Society of America, p. 5-25.
- Davis, G., 1999, *Structural Geology of the Colorado Plateau Region of Southern Utah, With Special Emphasis on Deformation Bands*: Boulder, CO, Geological Society of America.
- Downey, M. W., 1984, Evaluating seals for hydrocarbon accumulations: *The American Association of Petroleum Geologists Bulletin*, v. 68, p. 1752-1763.
- Fossen, H., and J. Hesthammer, 1997, Geometric analysis and scaling relations of deformation bands in porous sandstone: *Journal of Structural Geology*, v. 19, p. 1479-1493.
- Fowles, J., and S. Burley, 1994, Textural and permeability characteristics of faulted, high porosity sandstones: *Marine and Petroleum Geology*, v. 11, p. 608-622.
- Friedman, M., and J. Logan, 1973, Lüders' bands in experimentally deformed sandstone and limestone: *Geological Society of America Bulletin*, v. 84, p. 1465-1476.
- Goodwin, L., and W. Haneberg, 1996, Deformational fabrics and inferred permeability of faulted sands from the Rio Grande rift, New Mexico: *Geological Society of America Abstracts with Programs*, v. 28: A-255.

- Handschy, J., B. Jolley, and G. McRae, 1995, Fault seal mechanisms in contractional and transpressional settings: examples from the Ventura Basin, Southern California: ABSTRACT: American Association of Petroleum Geologists Bulletin, v. 79, p. 38.
- Hardmann, R. F. P., and J. E. Booth, 1991, The significance of normal faults in the exploration and production of North Sea hydrocarbons, in A. M. Roberts, G. Yielding, and B. Freeman, eds., The geometry of normal faults: Geological Society Special Publication No. 56, p. 1-13.
- Heald, M., 1956, Cementation of Simpson Group and St. Peter Sandstones in parts of Oklahoma, Arkansas, and Missouri: Journal of Geology, v. 64, p. 16-30.
- Heath, R. C., 1984, Groundwater regions of the U.S.: United States Geological Survey Water-Supply Paper 2242.
- Heynekamp, M., L. Goodwin, and P. Mozley, 1999, Controls on fault-zone architecture in poorly lithified sediments, Rio Grande Rift, New Mexico: implications for fault-zone permeability and fluid flow., in W. Haneberg, P. Mozley, J. C. Moore, and L. Goodwin, eds., Faults and Subsurface Fluid Flow in the Shallow Crust, Washington, D.C., American Geophysical Union, p. 27-49.
- Hippler, S., 1993, Deformation microstructures and diagenesis in sandstone adjacent to an extensional fault: Implications for the flow and entrapment of hydrocarbons: American Association of Petroleum Geologists Bulletin, v. 77, p. 625-637.
- Hippler, S., 1997, Microstructures and Diagenesis in North Sea Fault Zones: Implications for Fault-Seal Potential and Fault-Migration Rates, in R. Surdam, ed., Seals, traps, and the petroleum system: AAPG Memoir 67, p. 85-101.
- Hong, S.-h., 1999, Anisotropic Hydraulic Conductivity of Faulted Poorly Consolidated Eolian Sands: Bosque, New Mexico: MS thesis, New Mexico Institute of Mining and Technology, Socorro, New Mexico, 70 p.
- Horton, R., 1997, Tectonically controlled diagenesis of immature sandstone in the Western San Joaquin Basin, California: ABSTRACT: AAPG Pacific Section Meeting, p. 687.
- Jamison, W., and D. Stearns, 1982, Tectonic deformation of Wingate sandstone, Colorado National Monument: American Association of Petroleum Geologists Bulletin, v. 66, p. 2584-2608.

- Kelley, V., 1982, The right-relayed Rio Grande Rift, Taos to Hatch, New Mexico, in J. Grambling, and S. Wells, eds., New Mexico Geological Society Thirty-Third Annual Field Conference, Albuquerque, New Mexico Geological Society, p. 147-151.
- Knipe, R. J., 1993, The influence of fault zone processes and diagenesis on fluid flow, in A. D. Horbury, and A. G. Robinson, eds., Diagenesis and Basin Development, American Association of Petroleum Geologists, Studies in Geology #36, p. 135-148.
- Knott, S., 1993, Fault Seal Analysis in the North Sea: American Association of Petroleum Geologists Bulletin, v. 77, p. 778-792.
- Lozinsky, R., J. Hawley, and D. Love, 1991, Geologic overview and Pliocene-Quaternary history of the Albuquerque basin, central New Mexico, in B. Julian, and J. Zidek, eds., Field guide to geologic excursions in New Mexico and adjacent areas of Texas and Colorado, Socorro, New Mexico, New Mexico Bureau of Mines and Mineral Resources, p. 192.
- Machette, M., 1982, Quaternary and Pliocene faults in the La Jencia and southern part of the Albuquerque-Belen Basins, New Mexico: Evidence of fault history from fault-scarp morphology and Quaternary geology., in N. M. G. Society, ed., New Mexico Geological Society Guidebook - Albuquerque Country II, p. 161-169.
- Mair, K., I. Main, and S. Elphick, 2000, Sequential growth of deformation bands in the laboratory: Journal of Structural Geology, v. 22, p. 25-42.
- Maltman, A. J., 1994, The Geological Deformation of Sediments: New York, Chapman & Hall, 362 p.
- Marone, C., and C. Scholz, 1989, Particle-size distribution and microstructures within simulated fault gouge: Journal of Structural Geology, v. 11, p. 799-814.
- Menendez, B., W. Zhu, and T.-F. Wong, 1996, Micromechanics of brittle faulting and cataclastic flow in Berea sandstone: Journal of Structural Geology, v. 18, p. 1-16.
- Mollema, P. N., and M. A. Antonellini, 1996, Compaction bands: a structural analog for anti-mode I cracks in aeolian sandstone: Tectonophysics, v. 267, p. 209-228.
- Mozley, P., 1999, Elements of Sedimentary Petrography.
- Mozley, P., and L. Goodwin, 1995, Patterns of cementation along a Cenozoic normal fault: a record of paleoflow orientations: Geology, v. 23, p. 539-542.

- Muhlhaus, H. B., and I. Vardoulakis, 1988, The thickness of shear bands in granular materials: *Geotechnique*, v. 38, p. 271-284.
- Nybakken, S., 1991, Sealing fault traps--an exploration concept in a mature petroleum province: Tampen Spur, northern North Sea: *First Break*, v. 9, p. 209-222.
- Petit, J. P., 1987, Criteria for the sense of movement on fault surfaces in brittle rocks: *Journal of Structural Geology*, v. 9, p. 597-608.
- Pittman, E. D., 1981, Effect of fault-related granulation on porosity and permeability of quartz sandstones, Simpson Group (Ordovician), Oklahoma: *American Association of Petroleum Geologists Bulletin*, v. 65, p. 2381-2387.
- Pittman, E. D., and R. E. Larese, 1991, Compaction of lithic sands: experimental results and applications: *American Association of Petroleum Geologists Bulletin*, v. 75, p. 1279-1299.
- Porter, K. W., and R. J. Weimer, 1982, Diagenetic sequence related to structural history and petroleum accumulation: Spindle Field, Colorado: *American Association of Petroleum Geologists Bulletin*, v. 66, p. 2543-2560.
- Riedel, W., 1929, Zur mechanik geologischer Brucherscheinungen (ein beitrage zum problem der fiederspatten): *Zentralblatt für Mineralogie, Geologie und Paläontologie, Abhandlung B*, v. 1929B, p. 354-368.
- Russell, L., and S. Snelson, 1994, Structural style and tectonic evolution of the Albuquerque Basin Segment of the Rio Grande Rift, New Mexico, U.S.A., in S. Landon, ed., *Interior Rift Basins: AAPG Memoir 59*, Tulsa, OK, American Association of Petroleum Geologists, p. 205-258.
- Sanford, A., 1978, Characteristics of Rio Grande Rift in vicinity of Socorro, New Mexico, from geophysical studies, in J. Hawley, ed., *Guidebook to Rio Grande rift in New Mexico and Colorado*, Socorro, New Mexico Bureau of Mines and Mineral Resources, p. 241.
- Sigda, J. M., 1997, Effects of small-displacement faults on the permeability distribution of poorly consolidated Santa Fe Group sands, Rio Grande Rift New Mexico.: MS thesis, New Mexico Institute of Mining and Technology, Socorro, NM.
- Sigda, J. M., L. B. Goodwin, P. S. Mozley, and J. L. Wilson, 1999, Permeability alteration in small-displacement faults in poorly consolidated sediments: Rio Grande Rift, central New Mexico, in W. C. Haneberg, P. S. Mozley, J. C. Moore, and L. B. Goodwin, eds., *Faults and Subsurface Fluid Flow in the Shallow Crust* AGU Monograph 113.

- Smith, D. A., 1980, Sealing and non-sealing faults in the Louisiana Gulf Coast Salt Basin: AAPG Bulletin, v. 64, p. 145-172.
- Stanley, S., 1989, Earth and Life Through Time: New York, Freeman, 689 p.
- Steen, O., and A. Andresen, 1999, Effects of lithology on geometry and scaling of small faults in Triassic sandstones, East Greenland: Journal of Structural Geology, v. 21, p. 1351-1368.
- Swierczewska, A., and K. Antoni., 1998, Deformation bands and the history of folding in the Magura nappe, Western Outer Carpathians (Poland): Tectonophysics, v. 297, p. 73-90.
- Tchalenko, J., 1970, Similarities between shear zones of different magnitudes: GSA Bulletin, v. 81, p. 1625-1640.
- Underhill, J., and N. Woodcock, 1987, Faulting mechanisms in high-porosity sandstones; New Red Sandstone, Arran, Scotland, in R. Preston, and M. Jones, eds., Deformation of Sediments and Sedimentary Rocks, Geological Society of America, p. 91-105.
- Walsh, J. J., and J. Watterson, 1991, Geometric and kinematic coherence and scale effects in normal fault systems, in A. M. Roberts, G. Yieldgin, and B. Freeman, eds., The geometry of normal faults. Geological Society Special Publication 56, p. 193-203.
- Wilson, M. D., and E. D. Pittman, 1977, Authigenic clays in sandstones: recognition and influence on reservoir properties and paleoenvironmental analysis: Journal of Sedimentary Petrology, v. 47, p. 3-31.
- Wong, T.-f., C. David, and W. Zhu, 1997, The transition from brittle faulting to cataclastic flow in porous sandstones: Mechanical deformation: Journal of Geophysical Research, v. 102, p. 3009-3025.
- Worden, R., M. Mayall, and I. Evans, 2000, The effect of ductile-lithic sand grains and quartz cement on porosity and permeability in Oligocene and Lower Miocene clastics, South China Sea: prediction of reservoir quality.: AAPG Bulletin, v. 84, p. 345-359.
- Yielding, G., B. Freeman, and D. T. Needham, 1997, Quantitative Fault Seal Prediction: American Association of Petroleum Geologists Bulletin, v. 81, p. 897-917.

APPENDIX A: Samples Used for Point Count Analysis

Key:

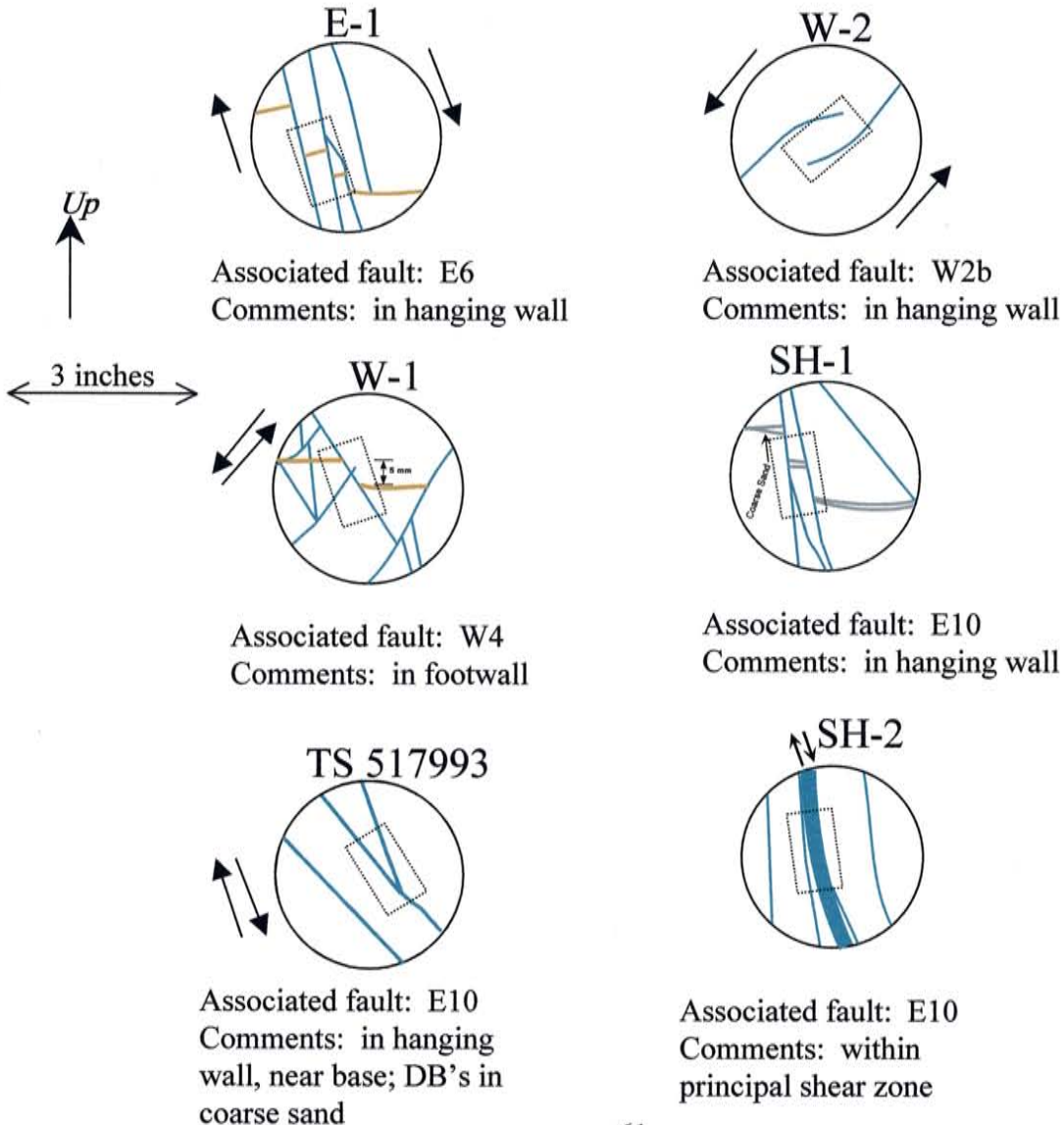
Each circular sketch represents a cross section of the cylindrical sample drilled from the outcrop.

Blue lines represent deformation bands, orange lines represent clay laminae, and grey lines represent stringers of coarse sand.

Arrows show direction of relative displacement.

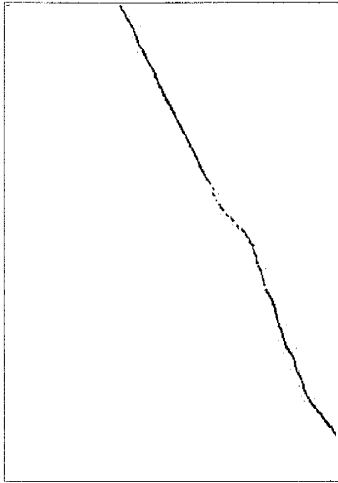
Dashed rectangles show the approximate orientation of the thin sections cut from each sample.

Fault names refer to surveyed fault ID in Figure 4.

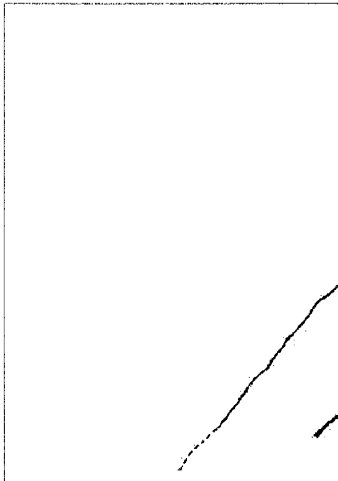


APPENDIX B: Fault Panel Sketches

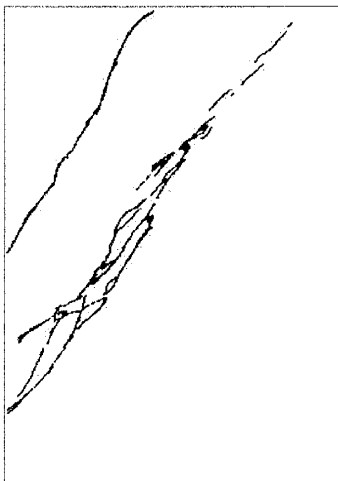
This appendix contains the 1:10 outcrop sketch panels for the west side of the Canyon Trail exposure. The table to the right of each sketch lists results from the image analysis routines. The number listed in the “Associated fault” row refers to ID of surveyed fault zones shown in Figure 4. Panel orientations (strike followed by dip) are given in degrees. Panel location comments note the position of the panel relative to surveyed faults or other panels (LRC = lower right corner of panel).



Panel ID:	1
Associated fault:	
Percentage DB material (%):	0.65
Number of intersections:	0
Number of segments:	5
Dominant segment dip (degrees):	62 N
# intersections / total segment length:	0
Panel location	LRC 1.27m south of W1
Panel orientation	24, 87 E



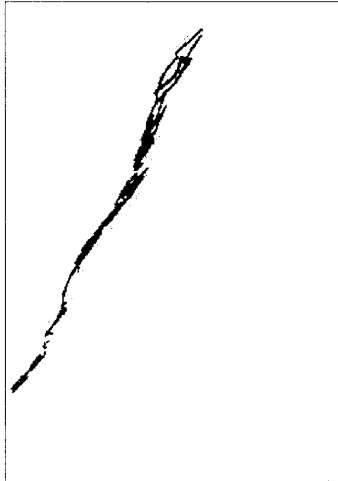
Panel ID:	3
Associated fault:	1
Percentage DB material (%):	.41
Number of intersections:	0
Number of segments:	4
Dominant segment dip (degrees):	51 S
# intersections / total segment length:	0
Panel location	LRC 15 cm north of W1
Panel orientation	26, 90



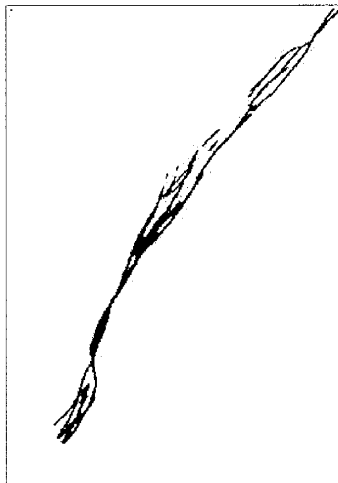
Panel ID:	4
Associated fault:	1
Percentage DB material (%):	2.28
Number of intersections:	22
Number of segments:	36
Dominant segment dip (degrees):	54 S
# intersections / total segment length:	3.47
Panel location	N of panel 3
Panel orientation	24, 90



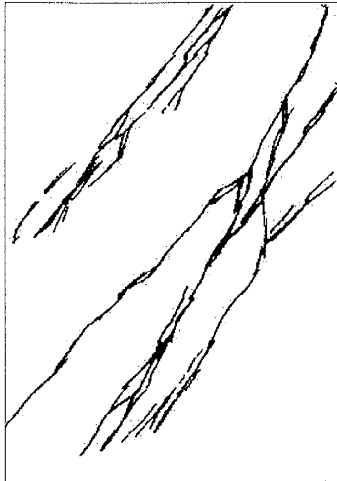
Panel ID:	5
Associated fault:	1
Percentage DB material (%):	.71
Number of intersections:	4
Number of segments:	8
Dominant segment dip (degrees):	58 S
# intersections / total segment length:	1.97
Panel location	Above panel 4
Panel orientation	24, 77 E



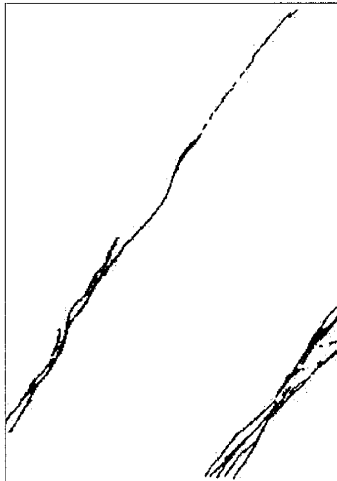
Panel ID:	6
Associated fault:	1
Percentage DB material (%):	1.8
Number of intersections:	16
Number of segments:	27
Dominant segment dip (degrees):	60 S
# intersections / total segment length:	4.94
Panel location	North of panel 5
Panel orientation	30, 76 E



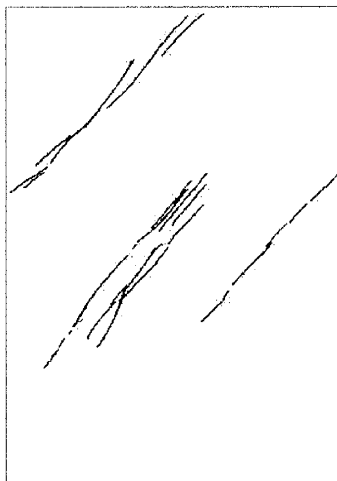
Panel ID:	7
Associated fault:	2
Percentage DB material (%):	2.53
Number of intersections:	22
Number of segments:	33
Dominant segment dip (degrees):	56 S
# intersections / total segment length:	5.06
Panel location	North of panel 6
Panel orientation	23, 78 E



Panel ID:	8
Associated fault:	2
Percentage DB material (%):	5.68
Number of intersections:	54
Number of segments:	88
Dominant segment dip (degrees):	56 S
# intersections / total segment length:	3.59
Panel location	North of panel 7
Panel orientation	23, 77 E



Panel ID:	9
Associated fault:	2
Percentage DB material (%):	2.42
Number of intersections:	22
Number of segments:	43
Dominant segment dip (degrees):	55 S
# intersections / total segment length:	3.73
Panel location	Above panel 8
Panel orientation	26, 76 E



Panel ID:	10
Associated fault:	2
Percentage DB material (%):	1.52
Number of intersections:	7
Number of segments:	30
Dominant segment dip (degrees):	56 S
# intersections / total segment length:	3.59
Panel location	North of panel 9
Panel orientation	15, 76 E



Panel ID:	11
Associated fault:	3
Percentage DB material (%):	6.29
Number of intersections:	19
Number of segments:	59
Dominant segment dip (degrees):	46 S
# intersections / total segment length:	0.98
Panel location	North of panel 10
Panel orientation	13, 73 E



Panel ID:	12
Associated fault:	3
Percentage DB material (%):	15.32
Number of intersections:	89
Number of segments:	146
Dominant segment dip (degrees):	43 S
# intersections / total segment length:	3.08
Panel location	North of panel 11
Panel orientation	15, 76 E



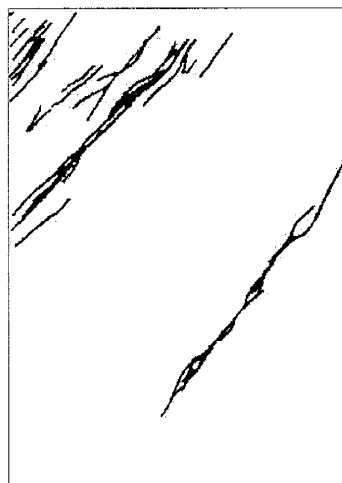
Panel ID:	13
Associated fault:	3
Percentage DB material (%):	7.42
Number of intersections:	30
Number of segments:	81
Dominant segment dip (degrees):	49 S
# intersections / total segment length:	1.64
Panel location	North of panel 12
Panel orientation	27, 73 E



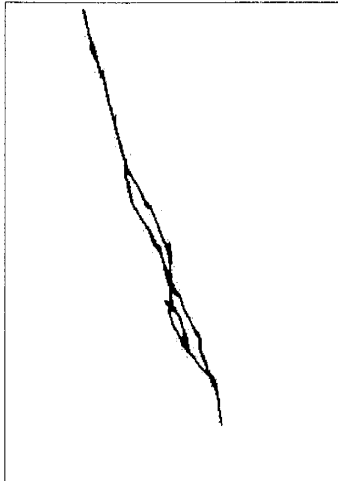
Panel ID:	14
Associated fault:	4
Percentage DB material (%):	7.53
Number of intersections:	31
Number of segments:	87
Dominant segment dip (degrees):	48 S
# intersections / total segment length:	1.56
Panel location	North of panel 13
Panel orientation	24, 65 E



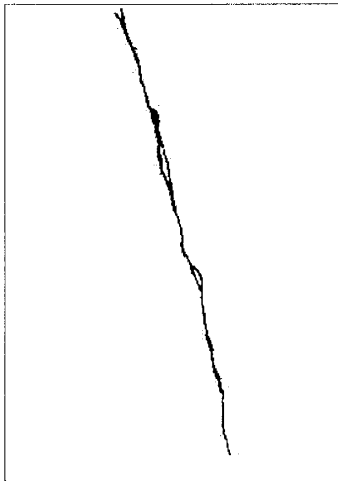
Panel ID:	15
Associated fault:	4
Percentage DB material (%):	9.51
Number of intersections:	55
Number of segments:	118
Dominant segment dip (degrees):	50 S
# intersections / total segment length:	2.63
Panel location	North of panel 14
Panel orientation	23, 71 E



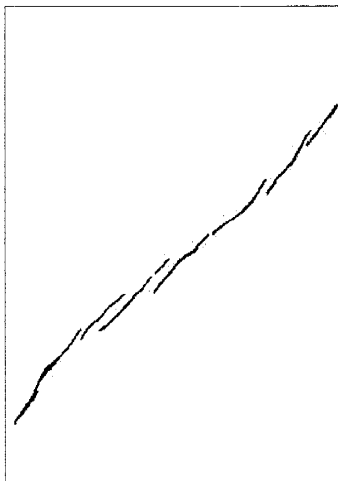
Panel ID:	16
Associated fault:	4
Percentage DB material (%):	4.18
Number of intersections:	30
Number of segments:	49
Dominant segment dip (degrees):	50 S
# intersections / total segment length:	3.71
Panel location	N. and 10 cm up from 15
Panel orientation	15, 75 E



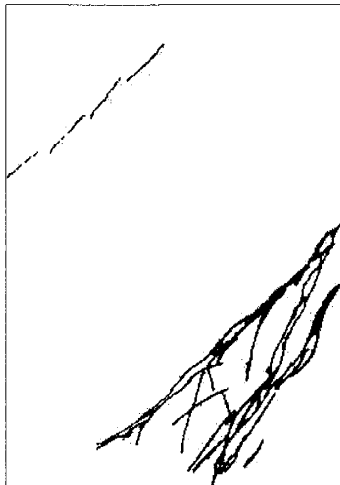
Panel ID:	17
Associated fault:	
Percentage DB material (%):	1.57
Number of intersections:	7
Number of segments:	12
Dominant segment dip (degrees):	73 N
# intersections / total segment length:	2.07
Panel location	80 cm N. of panel 16
Panel orientation	26, 74 E



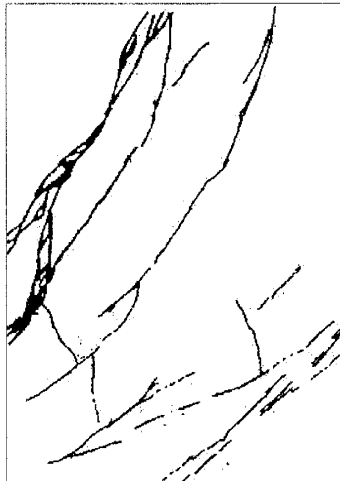
Panel ID:	18
Associated fault:	
Percentage DB material (%):	1.09
Number of intersections:	4
Number of segments:	6
Dominant segment dip (degrees):	76 N
# intersections / total segment length:	1.86
Panel location	3.63 m N of panel 17
Panel orientation	24, 76 E



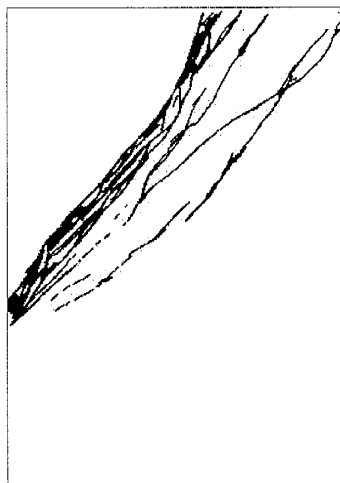
Panel ID:	19
Associated fault:	5
Percentage DB material (%):	1.01
Number of intersections:	0
Number of segments:	8
Dominant segment dip (degrees):	41 S
# intersections / total segment length:	0.0
Panel location	6.3 m N of panel 18
Panel orientation	26, 78 E



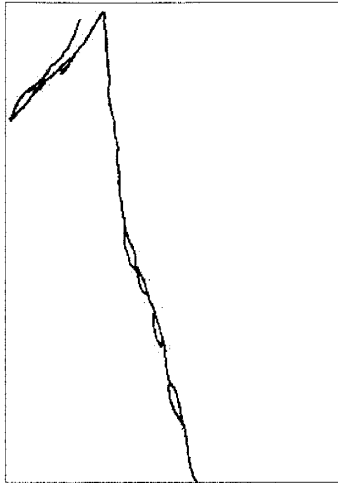
Panel ID:	20
Associated fault:	5
Percentage DB material (%):	4.4
Number of intersections:	40
Number of segments:	65
Dominant segment dip (degrees):	47 S
# intersections / total segment length:	4.55
Panel location	North of panel 19
Panel orientation	24, 80 E



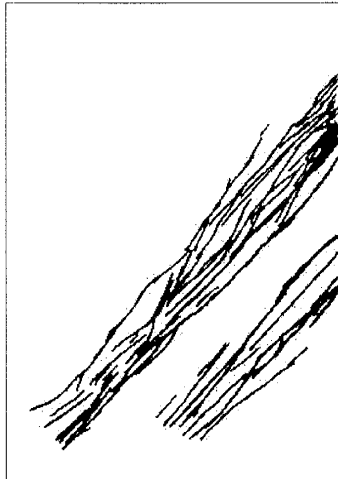
Panel ID:	21
Associated fault:	5
Percentage DB material (%):	5.41
Number of intersections:	46
Number of segments:	99
Dominant segment dip (degrees):	57 S
# intersections / total segment length:	3.16
Panel location	North of panel 20
Panel orientation	25, 75 E



Panel ID:	22
Associated fault:	5
Percentage DB material (%):	5.53
Number of intersections:	55
Number of segments:	84
Dominant segment dip (degrees):	52 S
# intersections / total segment length:	5.06
Panel location	North of panel 21
Panel orientation	27, 71 E



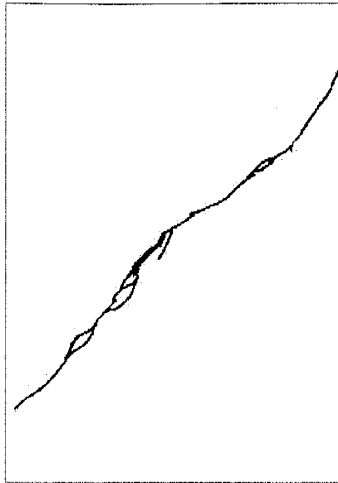
Panel ID:	23
Associated fault:	5
Percentage DB material (%):	1.54
Number of intersections:	13
Number of segments:	18
Dominant segment dip (degrees):	80 N
# intersections / total segment length:	3.65
Panel location	N. and 20cm up from 22
Panel orientation	31, 76 E



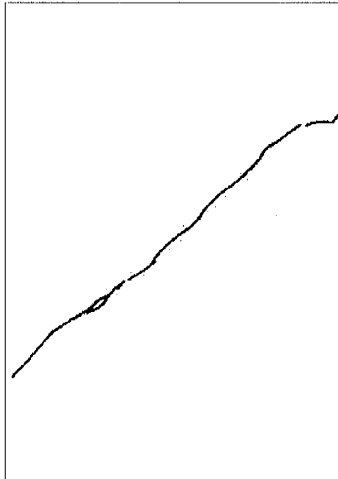
Panel ID:	24
Associated fault:	6
Percentage DB material (%):	9.47
Number of intersections:	72
Number of segments:	115
Dominant segment dip (degrees):	49 S
# intersections / total segment length:	3.46
Panel location	1.1 m N of 23
Panel orientation	39, 67 E



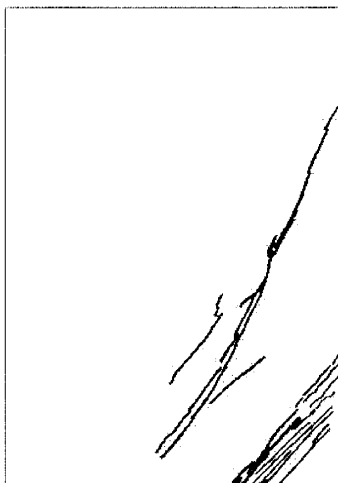
Panel ID:	25
Associated fault:	6
Percentage DB material (%):	5.45
Number of intersections:	32
Number of segments:	56
Dominant segment dip (degrees):	49 S
# intersections / total segment length:	3.04
Panel location	North of panel 24
Panel orientation	41, 72 E



Panel ID:	26
Associated fault:	
Percentage DB material (%):	1.23
Number of intersections:	9
Number of segments:	10
Dominant segment dip (degrees):	45 S
# intersections / total segment length:	4.05
Panel location	6.7 m N of panel 25
Panel orientation	39, 61 E



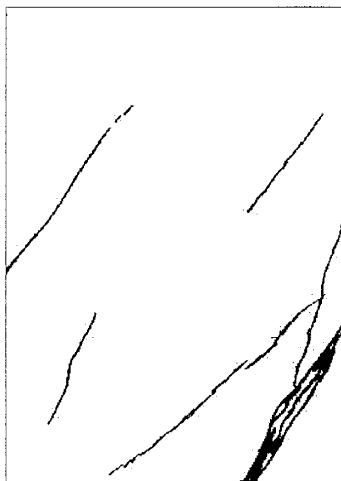
Panel ID:	27
Associated fault:	
Percentage DB material (%):	0.79
Number of intersections:	2
Number of segments:	5
Dominant segment dip (degrees):	42 S
# intersections / total segment length:	1.12
Panel location	N and 20cm up from 26
Panel orientation	43, 64 E



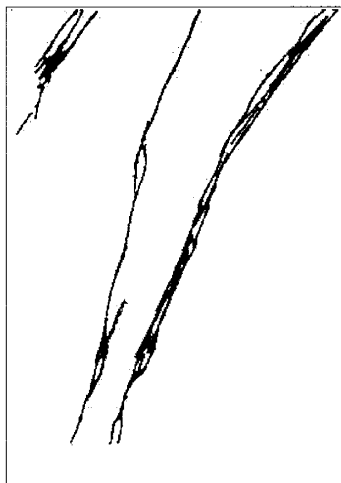
Panel ID:	28
Associated fault:	7
Percentage DB material (%):	2.95
Number of intersections:	18
Number of segments:	37
Dominant segment dip (degrees):	48
# intersections / total segment length:	2.06
Panel location	4.2 m N of 27
Panel orientation	34, 59 E



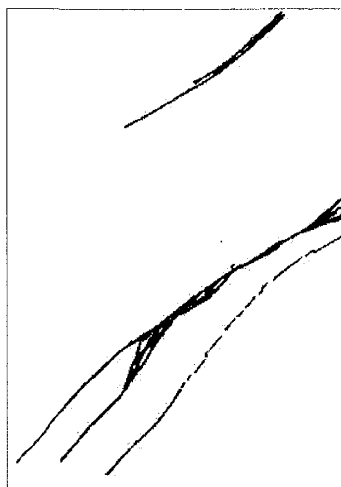
Panel ID:	29
Associated fault:	7
Percentage DB material (%):	7.03
Number of intersections:	48
Number of segments:	70
Dominant segment dip (degrees):	56 S
# intersections / total segment length:	4.1
Panel location	North of panel 28
Panel orientation	41, 65 E



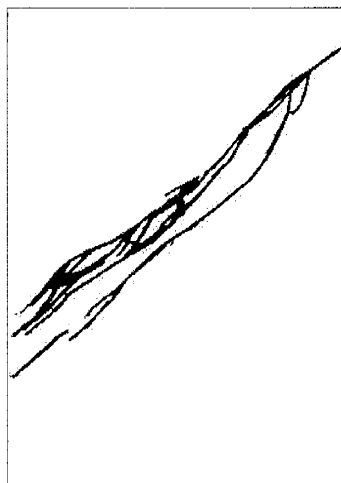
Panel ID:	30
Associated fault:	7
Percentage DB material (%):	2.83
Number of intersections:	19
Number of segments:	32
Dominant segment dip (degrees):	56 S
# intersections / total segment length:	2.88
Panel location	Above panel 29
Panel orientation	42, 84 E



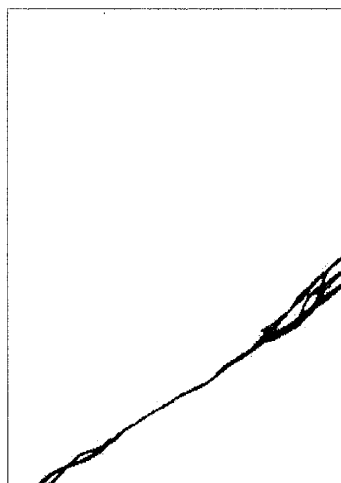
Panel ID:	31
Associated fault:	7
Percentage DB material (%):	4.55
Number of intersections:	33
Number of segments:	48
Dominant segment dip (degrees):	66 S
# intersections / total segment length:	3.91
Panel location	73 cm N of 30
Panel orientation	22, 85 W



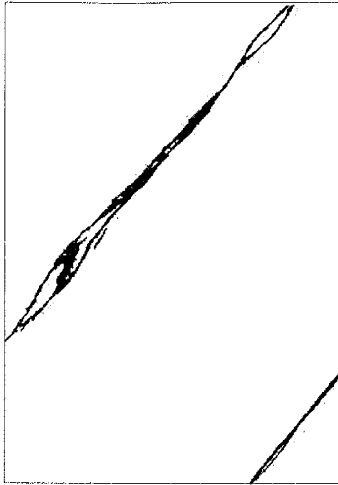
Panel ID:	32
Associated fault:	8
Percentage DB material (%):	2.96
Number of intersections:	16
Number of segments:	34
Dominant segment dip (degrees):	39 S
# intersections / total segment length:	2.79
Panel location	2.56 m N of 31
Panel orientation	31, 81E



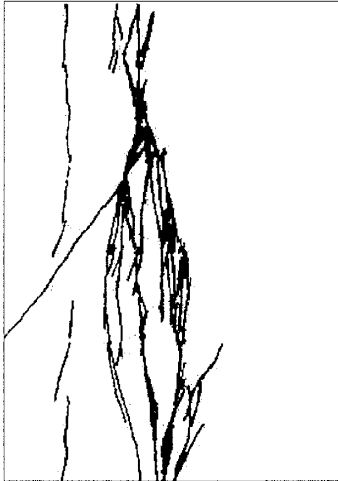
Panel ID:	33
Associated fault:	8
Percentage DB material (%):	4.32
Number of intersections:	23
Number of segments:	33
Dominant segment dip (degrees):	39 S
# intersections / total segment length:	3.81
Panel location	North of panel 32
Panel orientation	10, 32 E



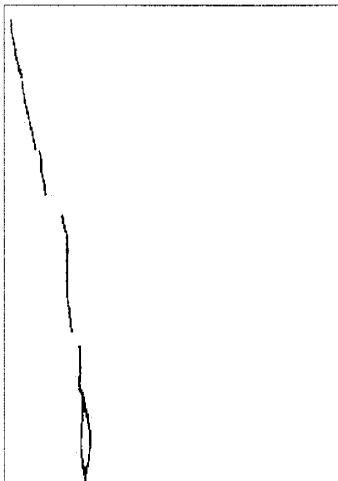
Panel ID:	34
Associated fault:	8
Percentage DB material (%):	1.83
Number of intersections:	11
Number of segments:	14
Dominant segment dip (degrees):	35 S
# intersections / total segment length:	4.01
Panel location	N and 1m above 33
Panel orientation	14, 64E



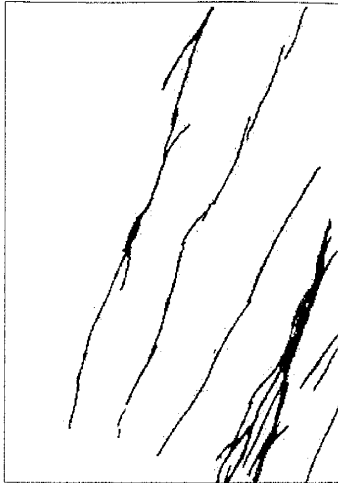
Panel ID:	35
Associated fault:	8
Percentage DB material (%):	2.51
Number of intersections:	22
Number of segments:	30
Dominant segment dip (degrees):	49 S
# intersections / total segment length:	4.91
Panel location	North of panel 34
Panel orientation	43, 68E



Panel ID:	36
Associated fault:	8
Percentage DB material (%):	7.67
Number of intersections:	55
Number of segments:	89
Dominant segment dip (degrees):	87 N
# intersections / total segment length:	3.39
Panel location	North of panel 35
Panel orientation	11, 62 E



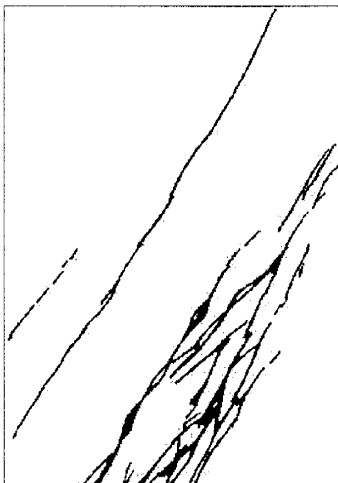
Panel ID:	37
Associated fault:	8
Percentage DB material (%):	0.75
Number of intersections:	2
Number of segments:	8
Dominant segment dip (degrees):	79 N
# intersections / total segment length:	0.68
Panel location	North of panel 36
Panel orientation	25, 56 E



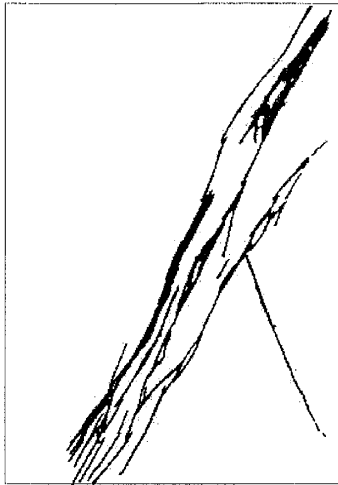
Panel ID:	38
Associated fault:	9
Percentage DB material (%):	4.86
Number of intersections:	21
Number of segments:	45
Dominant segment dip (degrees):	65 S
# intersections / total segment length:	1.83
Panel location	centered on W9
Panel orientation	40, 73 E



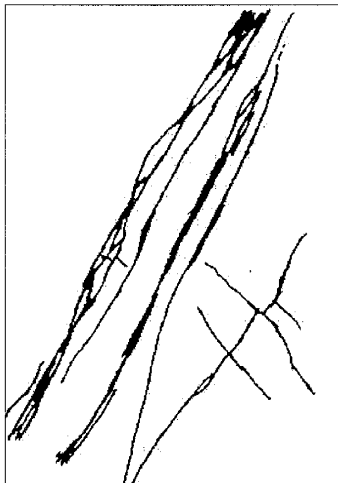
Panel ID:	39
Associated fault:	9
Percentage DB material (%):	4.58
Number of intersections:	30
Number of segments:	51
Dominant segment dip (degrees):	68 S
# intersections / total segment length:	2.6
Panel location	North of panel 38
Panel orientation	33, 63 E



Panel ID:	40
Associated fault:	9
Percentage DB material (%):	5.44
Number of intersections:	33
Number of segments:	65
Dominant segment dip (degrees):	56 S
# intersections / total segment length:	2.54
Panel location	Above panel 39
Panel orientation	15, 74 E



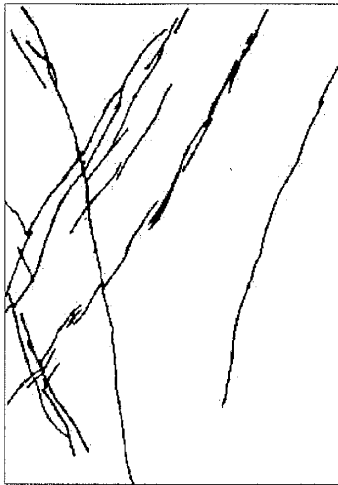
Panel ID:	41
Associated fault:	10
Percentage DB material (%):	6.49
Number of intersections:	30
Number of segments:	53
Dominant segment dip (degrees):	62 S
# intersections / total segment length:	2.97
Panel location	centered on W10a
Panel orientation	31, 78 E



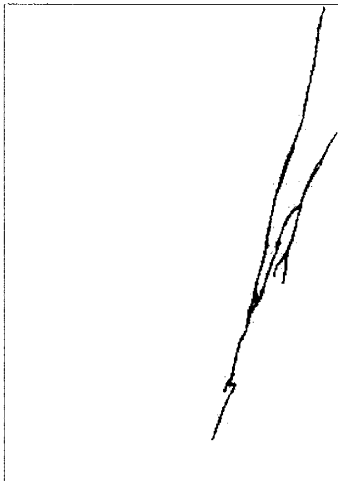
Panel ID:	42
Associated fault:	10
Percentage DB material (%):	7.46
Number of intersections:	48
Number of segments:	66
Dominant segment dip (degrees):	62 S
# intersections / total segment length:	3.53
Panel location	centered on W10b
Panel orientation	30, 82 E



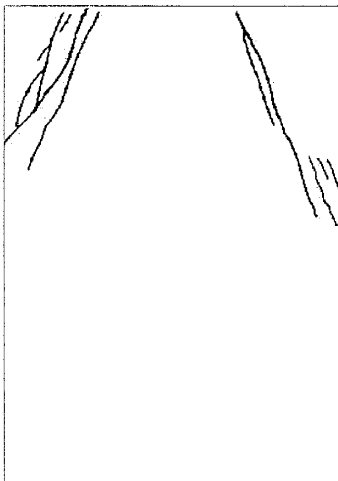
Panel ID:	43
Associated fault:	11
Percentage DB material (%):	12.19
Number of intersections:	134
Number of segments:	184
Dominant segment dip (degrees):	58 S
# intersections / total segment length:	5.8
Panel location	N and 40cm up from 42
Panel orientation	33, 83 E



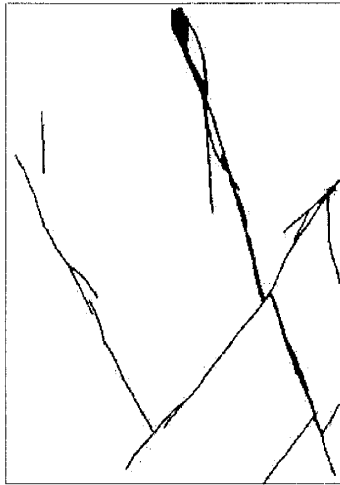
Panel ID:	44
Associated fault:	11
Percentage DB material (%):	5.35
Number of intersections:	34
Number of segments:	62
Dominant segment dip (degrees):	59 S
# intersections / total segment length:	2.34
Panel location	North of panel 43
Panel orientation	32, 78 E



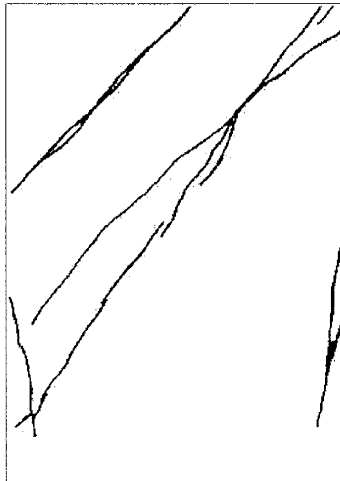
Panel ID:	45
Associated fault:	11
Percentage DB material (%):	1.47
Number of intersections:	5
Number of segments:	10
Dominant segment dip (degrees):	75 S
# intersections / total segment length:	1.38
Panel location	North of panel 44
Panel orientation	28, 83 E



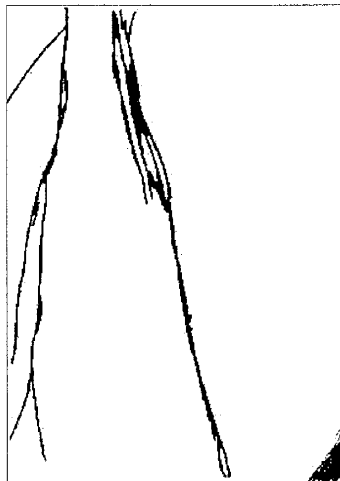
Panel ID:	46
Associated fault:	11
Percentage DB material (%):	1.48
Number of intersections:	5
Number of segments:	16
Dominant segment dip (degrees):	
# intersections / total segment length:	0.96
Panel location	North of panel 45
Panel orientation	27, 84 E



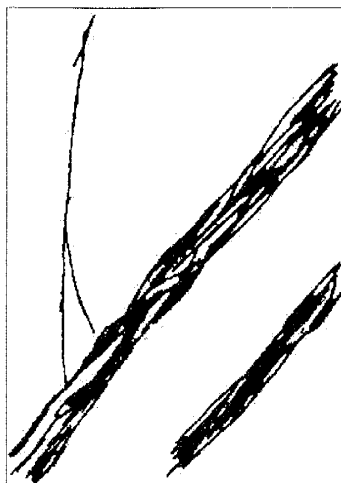
Panel ID:	47
Associated fault:	12
Percentage DB material (%):	3.59
Number of intersections:	18
Number of segments:	34
Dominant segment dip (degrees):	
# intersections / total segment length:	2.03
Panel location	1 m N. of panel 46
Panel orientation	31, 78 E



Panel ID:	48
Associated fault:	12
Percentage DB material (%):	2.99
Number of intersections:	8
Number of segments:	19
Dominant segment dip (degrees):	49 S
# intersections / total segment length:	1.21
Panel location	North of panel 47
Panel orientation	30, 70 E



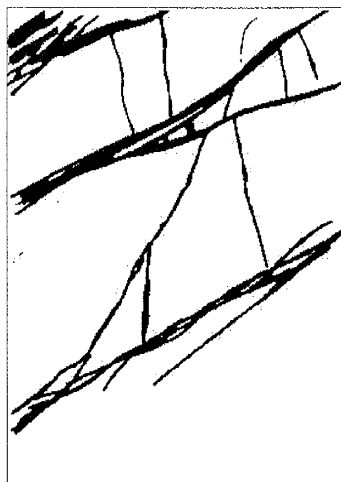
Panel ID:	49
Associated fault:	12
Percentage DB material (%):	4.75
Number of intersections:	25
Number of segments:	38
Dominant segment dip (degrees):	78 N
# intersections / total segment length:	2.61
Panel location	N and 20cm up from 48
Panel orientation	31, 77 E



Panel ID:	50
Associated fault:	13
Percentage DB material (%):	12.62
Number of intersections:	76
Number of segments:	92
Dominant segment dip (degrees):	48 S
# intersections / total segment length:	6.18
Panel location	North of panel 49
Panel orientation	38, 75 E



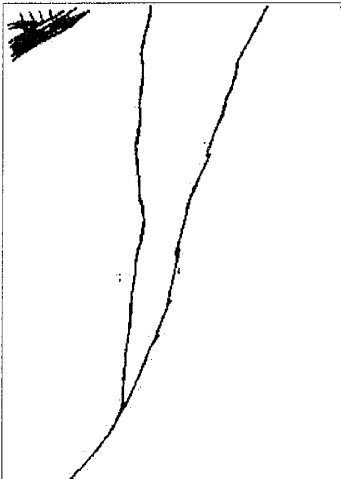
Panel ID:	51
Associated fault:	13
Percentage DB material (%):	20.0
Number of intersections:	125
Number of segments:	172
Dominant segment dip (degrees):	49
# intersections / total segment length:	5.57
Panel location	North of panel 50
Panel orientation	31, 78 E



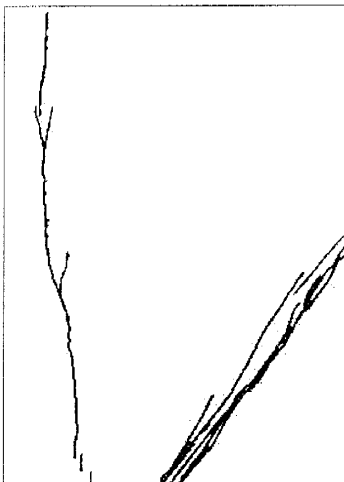
Panel ID:	52
Associated fault:	13
Percentage DB material (%):	11.31
Number of intersections:	52
Number of segments:	69
Dominant segment dip (degrees):	28 S
# intersections / total segment length:	4.72
Panel location	N. and 10cm up from 51
Panel orientation	10, 81 E



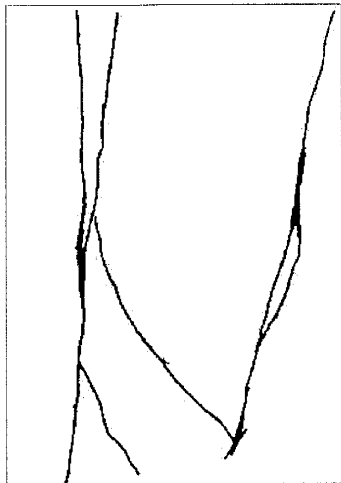
Panel ID:	53
Associated fault:	13
Percentage DB material (%):	11.32
Number of intersections:	89
Number of segments:	122
Dominant segment dip (degrees):	42 S
# intersections / total segment length:	5.55
Panel location	N. and 20cm up from 52
Panel orientation	26, 78 E



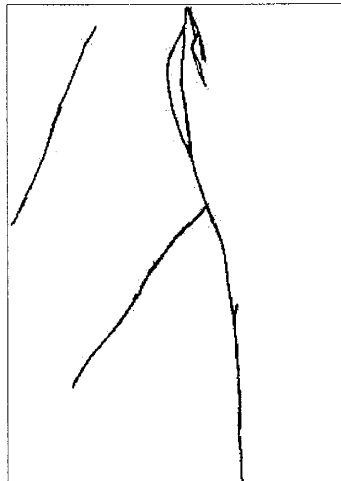
Panel ID:	54
Associated fault:	
Percentage DB material (%):	2.68
Number of intersections:	12
Number of segments:	17
Dominant segment dip (degrees):	74 S
# intersections / total segment length:	7.10
Panel location	North of panel 53
Panel orientation	24, 74 E



Panel ID:	55
Associated fault:	
Percentage DB material (%):	2.93
Number of intersections:	16
Number of segments:	27
Dominant segment dip (degrees):	54 S
# intersections / total segment length:	2.19
Panel location	57 cm N. of 54
Panel orientation	37, 68 E



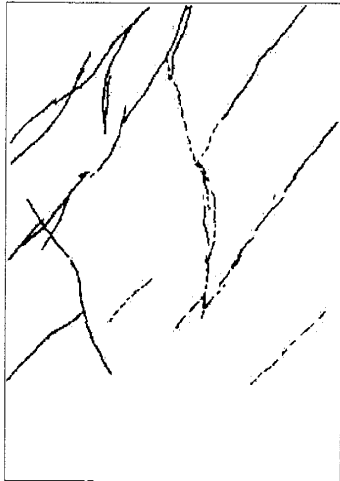
Panel ID:	56
Associated fault:	14
Percentage DB material (%):	3.57
Number of intersections:	8
Number of segments:	14
Dominant segment dip (degrees):	79 S
# intersections / total segment length:	1.11
Panel location	2.47m N. of 55
Panel orientation	25, 72 E



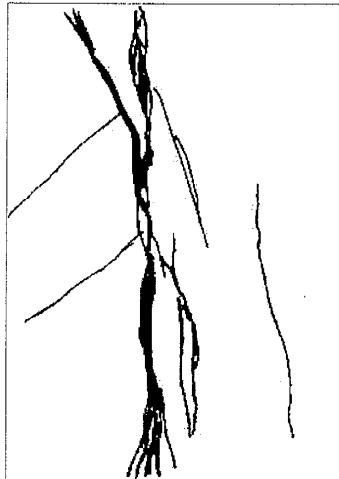
Panel ID:	57
Associated fault:	14
Percentage DB material (%):	2.21
Number of intersections:	6
Number of segments:	13
Dominant segment dip (degrees):	83 N
# intersections / total segment length:	1.27
Panel location	N. and 50cm up from 56
Panel orientation	20, 64 E



Panel ID:	58
Associated fault:	14
Percentage DB material (%):	12.28
Number of intersections:	57
Number of segments:	75
Dominant segment dip (degrees):	55 S
# intersections / total segment length:	4.05
Panel location	N. and 40cm down fr. 57
Panel orientation	30, 63 E



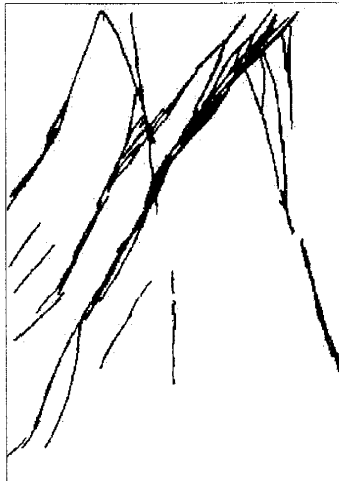
Panel ID:	59
Associated fault:	14
Percentage DB material (%):	3.21
Number of intersections:	17
Number of segments:	69
Dominant segment dip (degrees):	56 S
# intersections / total segment length:	1.75
Panel location	North of panel 58
Panel orientation	20, 67 E



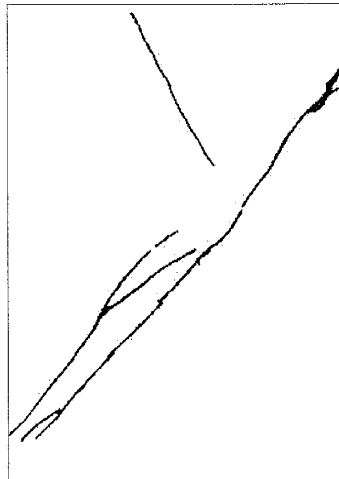
Panel ID:	60
Associated fault:	14
Percentage DB material (%):	6.44
Number of intersections:	45
Number of segments:	62
Dominant segment dip (degrees):	87 N
# intersections / total segment length:	4.14
Panel location	N. and 20cm above 59
Panel orientation	5, 64 E



Panel ID:	61
Associated fault:	W18
Percentage DB material (%):	13.26
Number of intersections:	83
Number of segments:	127
Dominant segment dip (degrees):	56 S
# intersections / total segment length:	3.82
Panel location	fault W18
Panel orientation	32, 53 E



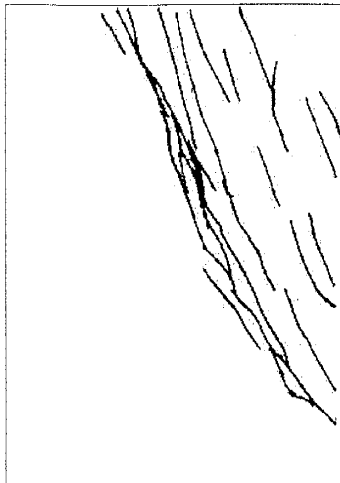
Panel ID:	62
Associated fault:	W18
Percentage DB material (%):	7.88
Number of intersections:	41
Number of segments:	66
Dominant segment dip (degrees):	59 S
# intersections / total segment length:	2.77
Panel location	North of panel 61
Panel orientation	50, 52 E



Panel ID:	63
Associated fault:	1.91
Percentage DB material (%):	4
Number of intersections:	11
Number of segments:	49 S
Dominant segment dip (degrees):	0.77
# intersections / total segment length:	
Panel location	2.1m N. of panel 62
Panel orientation	27, 65 E



Panel ID:	64
Associated fault:	
Percentage DB material (%):	4.82
Number of intersections:	28
Number of segments:	47
Dominant segment dip (degrees):	67 N
# intersections / total segment length:	2.51
Panel location	N. and 50cm up from 63
Panel orientation	21, 65 E



Panel ID:	65
Associated fault:	
Percentage DB material (%):	4.17
Number of intersections:	18
Number of segments:	36
Dominant segment dip (degrees):	68 N
# intersections / total segment length:	1.44
Panel location	North of panel 64
Panel orientation	21, 65 E